STUDY OF ENERGY ABSORPTION CHARACTERISTICS OF A THIN WALLED TUBE FILLED WITH CARBON NANO POLYURETHANE FOAM

A Thesis by

Damodar Goud Tankara

Bachelors of Engineering, Osmania University, 2007

Submitted to the Department of Mechanical Engineering
and the faculty of Graduate School of
Wichita State University
in partial fulfillment of
the requirements for the degree of
Master of Science

May 2011

STUDY OF ENERGY ABSORPTION CHARACTERISTICS OF A THIN WALLED TUBE FILLED WITH CARBON NANO POLYURETHANE FOAM

The fallowing faculty members have examined this final copy of this thesis report content, and recommend that it can be accepted in partial fulfillment of the requirements for the degree of Master of Science with a Mechanical Engineering as major.

_____
Hamid M Lankarani, Committee Chair

_____
Ramazan Asmatulu, Committee Member

_____
Krishna Krishnan, Committee Member

DEDICATION

To my Friends and Professor

ACKNOWLEDGEMENTS

I would like to thank every individual who made this thesis possible. First, I express gratitude to my thesis advisor, Dr. Hamid M Lankarani, for his scholarly and subtle support in my student life at Wichita State University. Without his support and supervision, this thesis work would have been impracticable. Next, I would also want to convey my appreciation and thanks to Dr. Ramazan Asmatulu and Dr. Krishna Krishnan for their effort and time in reviewing this manuscript. I want to extend my gratitude towards my parents, siblings and friends for their continuous support in all times of my life.

ABSTRACT

In last few decades much research work has been conducted on the development of most efficient crashworthy structures which can protect vehicle drivers, passengers or at least reduce the severity of the accident by absorbing kinetic impact energy in the event of an accident. Thin-walled tubes are most commonly used members as crashworthy structures. It has been shown that thin walled tubes, filled with foam materials, possess efficient energy-absorbing capability than the empty crashworthy structure. This characteristic of foam materials has led to the development of different new foam materials, which can absorb more impact energy. Nanotechnology is one of the emerging techniques used in development of advanced materials for engineering and other applications. One such application is in developing energy absorbing materials, which can be used in automotive and aerospace industry.

The purpose of this thesis is to analyze properties of the thin walled tubes with respect to energy absorption capacity, when filled with carbon nano-foam. The application of such carbon nano foam in the bumper area of a particular vehicle model namely Dodge Caravan is analyzed at different speeds. To accomplish this study, the Ls-Dyna code, a non-linear dynamic finite element solver is utilized. First, experiment using compression tests are carried out to obtain the behavior of the foam material by adding different weight percentages of carbon nano fibers. Next, the axial crushing behavior of thin walled steel tube was observed. The energy absorption capabilities of this crashworthy tube are tabulated and results are compared with rigid polyurethane foam under similar conditions. Finally carbon nano foam is applied in the bumper area of a vehicle model to study its crashworthy behavior in frontal impact at different speeds of the vehicle.

TABLE OF CONTENT

TABLE OF CONTENT (CONTINUED)

CHAPTER PAGE

LIST OF TABLES

LIST OF FIGURES

LIST OF FIGURES (Continued)

LIST OF FIGURES (Continued)

FIGURE PAGE

LIST OF ACRONYMS/NOMENCLATURE

A	Area under crush
ASTM	American Society for Testing and Materials
CG	Center of Gravity
CNF	Carbon nano fibers
CFR	Carbon fiber re-in forced
D	Diameter of tube
E	Elastic modulus
E_s	Specific energy absorption
f	Force
FE	Finite element
H	Hardness
K	Collapsibility
L	Length of the tube
LSTC	Livermore Software Technology Corporation
K	Stiffness
L_i	Initial crushing length
L_f	Final crushing length
m	mass of the specimen
NASA	National Aeronautics and Space Administration
NCAP	New Car Assessment Program
NHTSA	National Highway Traffic Safety Administration
P	Crushing load

P_m	Mean crush load
P_{max}	Maximum force
S	Slope
SEA	Specific energy absorption
T_n	Fundamental time period
V	Volume of crushed structure
W	Total energy absorbed
Δl	Change in length
δ_m	Penetration depth
ε	Strain
v	Poisson's Ratio
ρ	Density of the material
ρ_a	Actual density of the material
ρ_r	Relative density of the material
ρ_s	Strut density of the material
σ_m	Mean stress
σ_y	Yield stress
σ_u	Ultimate stress
v	Velocity

CHAPTER 1

INTRODUCTION

1.1 Crashworthiness and its Goals

Safety of the driver and the passenger has become an issue almost from the beginning of mechanized road vehicle development. The first crash event which was reported, was during the demonstration of a steam engine developed by Nicolas-Joseph Cugnot [1] in 1771. The earliest recorded automobile accident was on August 31, 1869 in Parsonstown, Ireland [1]. Since then, as the advancement in automotive technology improved, the number of accident and their severities were also increased. This automatically increased the importance over the safety of the driver and its passengers. This made automotive engineers to develop structures which can reduce or eliminate the effects of an accident on the occupant. Such structures are called as crashworthy structures and such property is being called as Crashworthiness [2]. The other way of defining crashworthiness is the ability of a structure to protect its occupants during an impact or the ability to absorb the impact energy and thereby bringing the passenger compartment to rest without the occupant being subjected to high or sudden decelerations, which can cause serious injuries in a survivable crash. Crashworthiness can be achieved and improved by controlled failure of the structure and reducing the load profile during crash. By considering these two factors thin walled tube structures become the most commonly used crashworthy elements.

The goal of crashworthiness is to develop an optimized vehicle structure that can absorb the kinetic crash energy by controlled vehicle deformations while maintaining adequate space so that the residual crash energy can be managed by the restraint systems to minimize crash loads transfer to the vehicle occupants. To satisfy these main objectives, over the years engineers developed different materials and by using these materials they developed body structures which

undergo progressive deformation to absorb the crash kinetic energy in the form of plastic deformation. And still, engineers are conducting research to improve crashworthy properties for vehicles which can provide occupant protection by maintaining its structural integrity of passenger compartment and it should simultaneously control the crash deceleration pulse to fall below the upper limit of human tolerance.

1.2 Crashworthiness and its Quantitative Measure

Crashworthiness can be quantitatively measured in terms of specific energy absorption (E_s) (SEA) which depends on type of material and this can be expressed as follows [3]

$$E_s = \frac{W}{V\rho} \tag{1.1}$$

where, W is the total energy absorbed,

V is the crushed structure volume

ρ is the density of the structure material

Equation (1.1) suggests that specific energy absorption can only be improved by decreasing the product of volume and density. This is the reason why thin walled tubes are most commonly used elements as crashworthy structures. Metals are being used as the material for these structures which fail under crush or impact through by plastic deformation i.e., either by buckling or by folding in a similar type fashion. The failure of thin walled tubes depends highly upon crush speed, triggers and geometry of the structure. These crashworthy structures are mostly are of axis-symmetric tubular structures in geometry, because of the easiness in production and being very close to actual geometry of the crashworthy members. So many experiments and plenty of investigation is being carried out to find out the energy absorption capabilities of metallic tubes under different conditions such as different cross sectional area, different materials as empty tubes, and foam filled tubes which are either metallic and non-

metallic foams. In this thesis an attempt is made to study and analyze the difference in the energy absorption for such thin walled tubes which are filled with a non-metallic crushable foam material.

1.3 Crashworthy Tubes

Tubular structures provide widest range of possible energy absorbing systems for any simple structure. Apart from their use as energy absorbers, their common existence as structural elements implies an in strict energy absorbing capability in the largest part of the vehicle structures. This double role is most desirable, predominantly in transport vehicle design where minimization of weight plays an important role.

Shells made of ductile materials can be subjected to a wide range of deformation modes and various loading conditions, as discussed by many researchers dealing with lateral compression or tube flattening, local loading of tubes, axial buckling and bending of circular cylindrical shells, square and rectangular tubes, conical shells and frusta, honeycomb material, tube inversion and sandwich plates. In recent years, it has been found that the thin walled steel tubes filled with foam materials posses more specific energy absorption capacity than other crashworthy tubes.

The optimization of a crashworthy structure depends on its composition, fabrication characters, and volume ratio of metal to composites. Depending on the material, crashworthiness can be represented in terms of specific energy absorption (E_s). Figure 1.1 shows the variation of an actual crush load with respect to the crush length. It shows that the crush load rises to a maximum value (peak load) in the beginning of crushing then drops after a certain point and remains constant from then on. The aim is to minimize the initial peak load so as to avoid large

energy being transferred to the occupant and increase the mean load to improve energy absorption capacity of that structure.

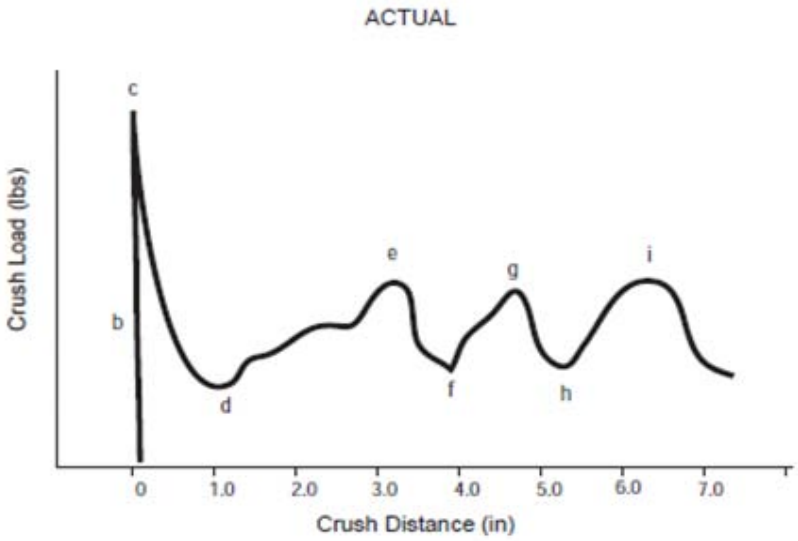

Figure 1.1 Actual load vs. displacement curve in axial crushing [2]

To study the behavior of this thin walled tubes an idealized method is utilized. Figure 1.2 shows the behavior of thin walled tubes where the sudden drop is eliminated by adding a triggered column.

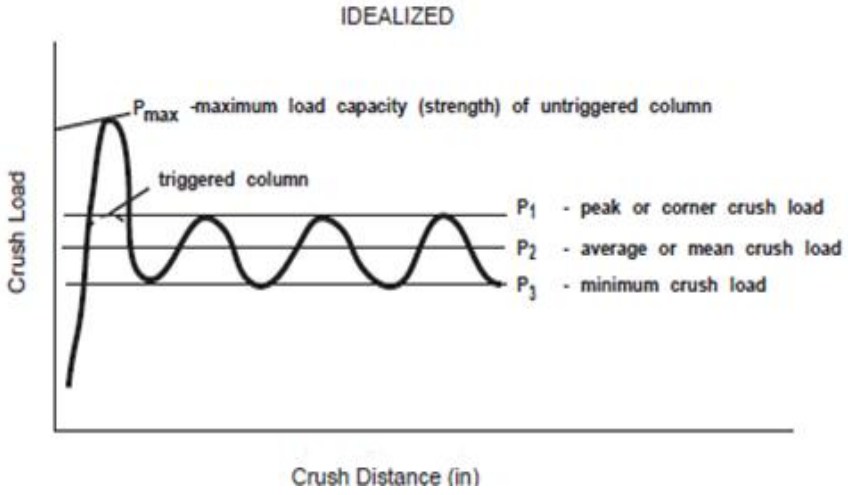

Figure 1.2 Idealized load vs. displacement curve in axial crushing [2]

1.4 Tabular Structures Testing Methods

There are number of methods are available to study the behavior tabular structures. Depending on the type of application and type of structure a particular testing method is used. Figure 1.3 shows a typical compression test setup with all necessary equipment.

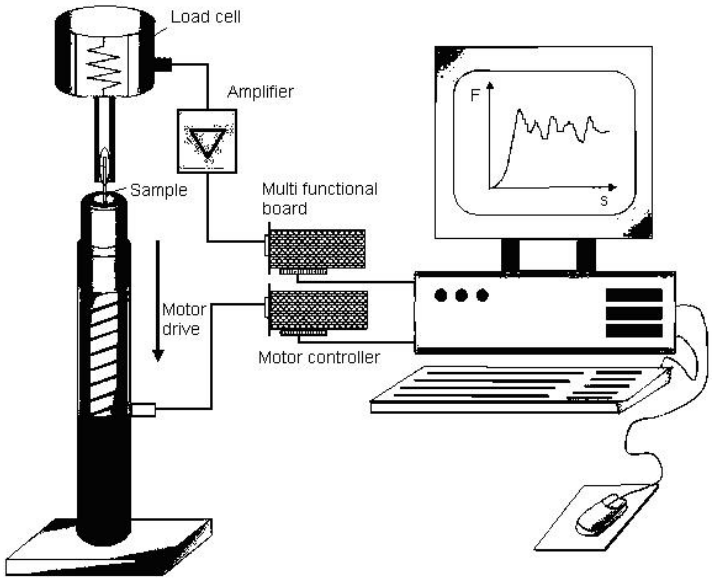

Figure 1.3 Typical Compression test set-up [3]

The classification of crush test/compression test is done based on the rate of loading and depending on this criterion there are mainly two types of tests namely quasi static and impact testing.

1.4.1 Quasi-static testing

Quasi-static means very slow process and this type of testing can be defined as the test which is carried out on the specimen at a constant speed of load, ranging between $1.5x10^{-3}$ m/s to 0.1 m/s [3]. The test specimen is compressed between two flat platens which are parallel to each other. One of them is stationary while the other will travel at a constant rate. The advantages of quasi-static tests are that the test can easily controlled and the equipment required is not very expensive when compared to any other forms of testing. Because of this reason quasi-static

testing has an edge over other types of testing. Figure 1.4 shows a typical compression testing machine set up, which consist of set of platens, one is fixed and the other moves in down-word direction crushing the specimen. This type of test cannot be considered as true simulation to the actual crash scenario as most of the materials are strain rate dependency. Even though materials show very good energy absorption after quasi-static testing, this test cannot convince that with actual crashworthy structures behavior. This is because the energy absorption ability of crashworthy structures significantly depends on the speed at which they are compressed.

Figure 1.4 Quasi-static test setup [3]

The force and displacements are measured using load cells and stain gauges. Compression data will be recorded manually or by using computers. The crucial part of the compression test is to select the appropriate load cell depending on the type of the material.

1.4.2 Impact testing

Impact testing or shock test is a type of test where the loading is sudden and the loading rate is much higher than the quasi static load, the required loading rate can be achieved by

dropping the given from a pre-calculated height. A schematic representation of drop impact testing is shown in Figure 1.5. The axis of the specimen is set to be parallel with the line of action of the load or the drop weight while it is mounted on the apparatus. Drop weight is positioned at a distance to gain the pre-calculated values of speed and impact energy and then experiment is carried out. Impact tests provide almost similar conditions to that of actual real time conditions of a crash event. Unlike quasi-static test, in this test strain rate effects of the test material is taken into consideration.

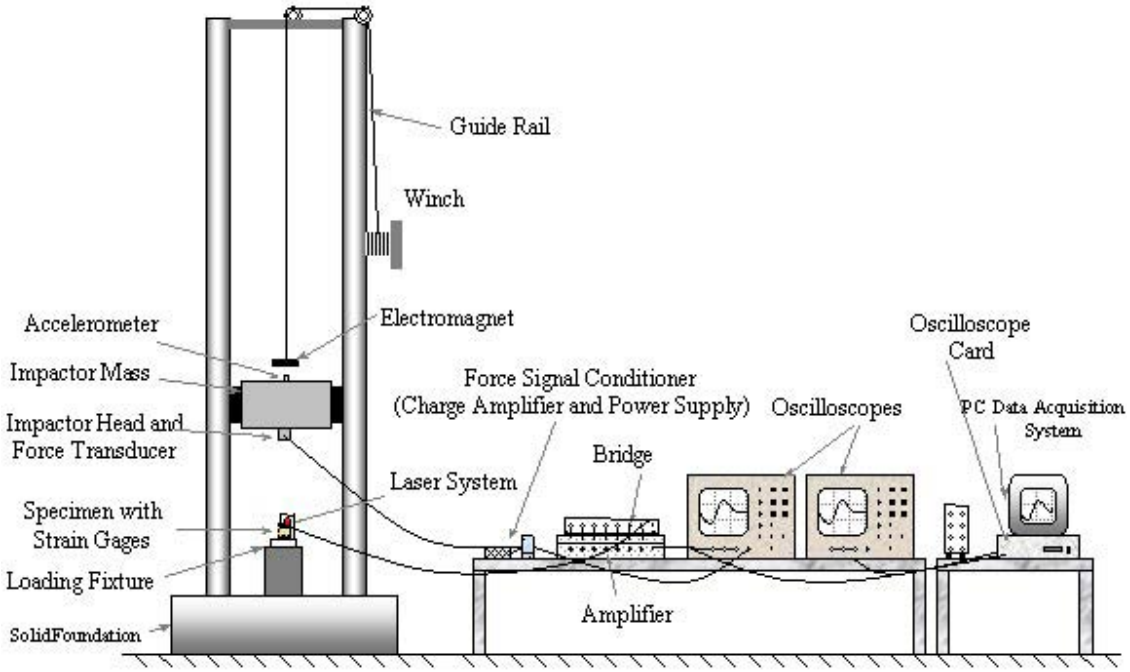

Figure 1.5 Impact test setup [3]

As the total time required for this test is very less, this test requires high speed camera, electronic controllers to collect the test data. Due to this requirement of additional equipment, impact test is an expensive test to carry. The Figure 1.5 shows several equipments which are used and required in the impact testing.

1.5 Specific Energy Absorption

The energy absorbed per unit mass of the material is defined as Specific energy absorption (SEA). To calculate SEA, first the amount of energy has to be calculated, which is the area under the load displacement curve with respect to Figure 1.1 and mathematically it can be written as [3]:

$$W = \int_0^l P \, . \, dl \tag{1.2}$$

where, W is the total energy absorbed during crushing

P is the crushing load and,

l is length of crushed portion

Assuming this crush behavior as progressive type for optimum conditions is given by

$$W = \int_{Li}^{Lf} P \, . \, ds = P_m \, (L_f - L_i) \tag{1.3}$$

where, P_m is the mean crush load

L_i is the initial length of the crushed portion of the specimen and

L_f is the final crushing length as shown in Figure 1.1.

The specific energy absorption E_s is given by

$$E_s = \frac{W}{m} \tag{1.4}$$

where, m is the mass of the specimen tube

combining equations (1.3) and (1.4), one obtains

$$E_s = \frac{W}{m} = \frac{P_m \, (L_f - L_i)}{V \, \rho} \tag{1.5}$$

where, V is the volume and

ρ is the density of the specimen tube material.

The Equation (1.5) can be expressed in terms of cross section area of tube (A) and length (L) as

$$E_s = \frac{W}{m} = \frac{P_m\,(L_f - L_i)}{V\,\rho} = \frac{P_m\,(L_f - L_i)}{A\,L\,\rho} \tag{1.6}$$

If L_i is very small when compared to L_f the Equation (16) can be written as

$$E_s = \frac{P_m\,.\,L_f}{A\,L\,\rho}$$

The ratio of L_f to L is called as "collapsibility of the specimen tube", which is denoted as K

$$K = \frac{L_f}{L} \tag{1.7}$$

and the ratio of P_m to A represents mean crush stress σ_{m} of the specimen tube. Now substituting K and σ_{m} in the Expression (1.7) one obtains an equation for E_s as fallows

$$E_s = \frac{\sigma_m\,.\,K}{\rho} \tag{1.8}$$

From Equation (1.8), it can be shown that the energy absorption capability of the specimen tube is a function of its mean stress and total energy absorbed is the area under the load-displacement curve.

1.6 Modes of Failures in Axial Crushing

When a tubular member is crushed axially, it undergoes deforms in different ways. These axial crushing deformation mechanisms are classified into three fundamental failure modes. Each mechanism explains how the tubular structure deforms in an axial loading and importance of these failure modes, assumptions made to represent these behavior in an analytical form.

1.6.1 Euler mode of buckling

Buckling occurs when thin walled tubes subjected to compressive loads, and it occurs in three different ways depending on its L/D ratio as shown in Figure 1.6. In this case the thin walled member also subjected to bending moment which reduces buckling load. In this type of failure, structural member moves laterally and shortens under compression and this mode depends on the length, thickness and the diameter of the structure. On the other hand automotive structures are designed such a way that there will not be any buckling and therefore this phenomenon is hardly seen in automotive structures.

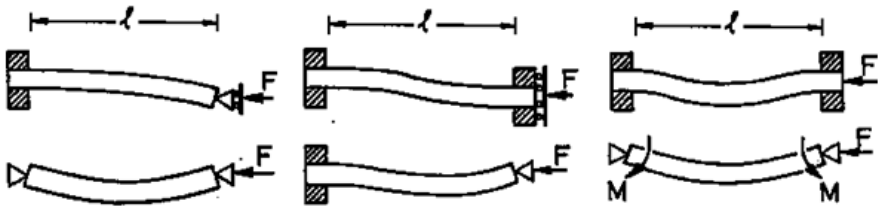

Figure 1.6 Buckling behavior of structure [4]

1.6.2 Progressive mode of crushing

This type of failure is the most common mode in automotive impacts and usually seen in tubes made up of elastic materials. This mechanism can also be observed in composite tabular structures where proper trigger mechanism is used. Figure 1.7 shows an ideal progressive crushing behavior of a tubular structure under axial loading conditions.

Figure 1.7 Progressive crushing in uni-axial loading mode [4]

Filling crushable materials will help the tubular structures to fail under progressive type pattern which absorbs more energy. The function of a trigger mechanism is to act as a pre-stressed location to initiate failure of the structure from a specific location while the function of a filler material is to absorb the energy and transfer it to the metallic structure during the impact. When compared to other modes of failures progressive crushing gives advantages like more energy absorption, low peak load value and min ratio of peak load to mean crush load when compared to structures failing catastrophically

1.6.3 Catastrophic mode of failure

When this type of failure occurs the load reaches to the peak value in a short period of time and this is followed by a sudden drop. As a result of these phenomenon, the structure fails by absorbing less energy. This type of failure occurs mostly in composite materials. In case of crashworthy structure design this mode of failure can be neglected.

1.7 Motivation and Objective

Engineers and researchers have been conducting research on different materials which can be used as core material in tabular structures. These filling materials will improve the energy absorption capabilities of tabular structures. Mamalis [5] et al and some other researchers had conducted research on rectangular tubular structure which were filled with poly-urethane foam and other metallic foams. They had concluded that the filling of poly-urethane and metallic foam materials will improve energy absorption capability of the structure by improving the failure mechanism of the tubular structure. The application (structural and for acoustics) of different foam materials (aluminum, poly-urethane, etc.,) in different areas of an automobile was shown in Figure 1.8. Materials is always been the most interesting and evolving topic for researchers and

nano technology gave more challenging task to many of the researchers who are working in this domain of research.

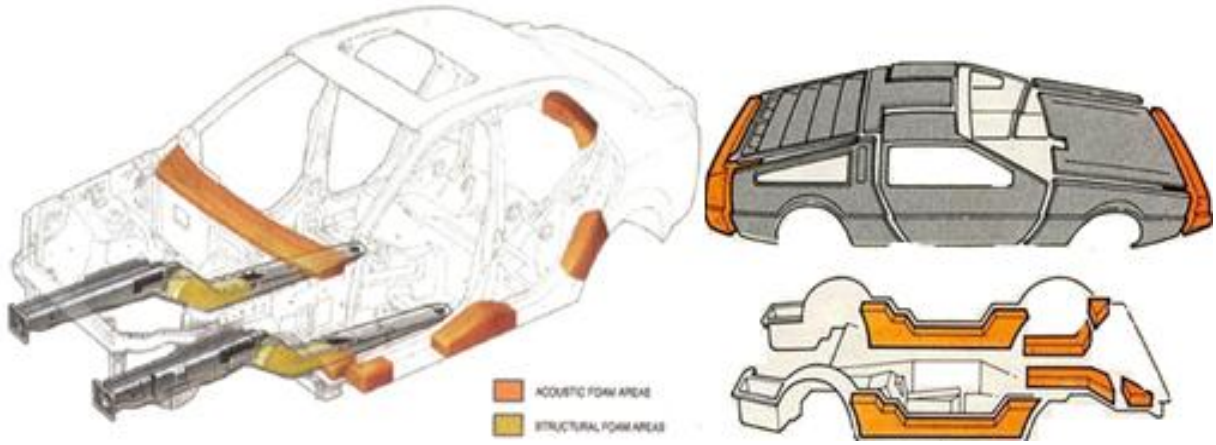

Figure 1.8 Application of foam materials in car structures [6]

Saha et al. [7] had conducted research on poly-urethane foam materials. Where he adding different nano particles to poly-urethane foam and found that the addition of carbon nano tubes will improve the mechanical and thermal properties to a significant amount. The main aim of this research work is to analyze the energy absorption characteristics of thin walled tubes when they are filled with carbon nano foam material. To achieve this first, study will be conducted on available foaming materials that are being used as core materials to compare carbon nano foam properties. Second, the effect of infusion of carbon nano particles into the polyurethane will be studied. Third, the analysis will be carried out to study the energy absorption characteristics of thin walled tubes filled with carbon nano poly urethane foam and fourth, the foam is being introduced into dodge caravan vehicle bumper to study its effect on energy absorption in a crash scenario. Finally, the results will be summarized and discussed from this analysis. Present Study was carried using LS-Dyna, an explicit dynamic finite element analysis code. Modeling was performed using Hypermesh and Ls-Prepost was used as a pre and post processing tool.

CHAPTER 2

LITERATURE SURVEY

2.1 Introduction

The safety of passengers, or in other words the survival from accidents is always been the primary challenging task to crashworthy engineers and this has led the researchers to focus their attention on designing such suitable mechanisms and systems that will function effectively to protect passengers [2, 5]. The secondary purpose of the crashworthiness engineer is to protect or to avoid considerable damage to the vehicle in case the collision is relatively small, i.e., vehicle crash with velocities lower than 15 km/h.

The function of crashworthy structures can easily be achieved by regulating the crushing behavior of the automotive structural parts. This can be achieved by strategically placing the energy absorbing components in the areas which are more prone to accidents. Figure 2.1 shows the arrangement of structural elements and these different structures were represented in different colors.

Figure 2.1 Typical representation of car energy absorbing structures in automobiles [8]

Tubes can be used as structural elements, which undergo deformations under bending, buckling and mostly under crushing. The crushing load is applied at one end (proximal end) of the tube and the other end (distal) supported by a stronger structure, then the behavior of the structural elements under this type of loading is similar that of compression under quasi-static conditions. The ability of each structural element to under this type of failure depends on the material, the geometrical characteristics and the pattern of deformation. The total stability of the tube is as important as its energy absorbing capacity and mean-crushing force [1, 5].

Researchers conducted many experiments on different cross sectional areas of thin-walled tubes and found that the rectangular cross sectional tubes are the most efficient and easily available structural elements, which are produced very easily [9]. Figure 2.2 shows detail of an aluminum square tube and a steel circular tube which were crushed axially. These tubular structures generally deform in two different ways and these deformations depend on their thickness (t), length (l), width (c) of the section. The first deformation type is a compact behavior, where the tube buckles by forming a series of contiguous folds, and the next is a non-compact behavior where the tube collapse by forming a series of folds which are separated by curved panel sections.

Figure 2.2 Cylindrical and square tubes under axial crushing [9,10]

Attention should be paid in the non-compact mode of deformation to avoid an Euler-type global instability or skewed deformations, which is a relatively inefficient energy absorbing mechanism. Under compression loads, the more thinner is the empty tube, the more irregular will be it's mode of collapse. Specifically, several circumferential buckles merged together to result as non axi-symmetric buckling mode which will lead to Euler buckling and consequently to loss its energy absorbing capacity. If this buckling behavior of the tube is changed to a progressive behavior, it can absorb a large amount of the compression or crushing energy. The buckling behavior of the tubes can be changed to a progressive collapse mode by filling crashworthy structures with a filler material. This is the reason researchers directed their work to analyze the behavior of sheet metal tubes reinforced with compressible filler materials to provide more efficient mechanisms of collapse with regard to the stability and the absorbing energy capacity [1,3,6].

2.2 Effect of Reinforcement of Tubes

The main function of the filler materials is to strengthen the structure and it should also improve the energy absorbing capacity by creating more efficient mechanism of collapse with respect to the stability and the absorbing capacity. The filler material should not increase the overall weight of the structure as weight is an important design factor which has to be considered in any transportation industry. Many researchers did lot of work in studying the effect of filling the tabular structures with some reinforcement material. Mamalis et al. in 1991 [5] were the first to study bi-metallic tubes comprising of composites and metals such as aluminum and steel. Figure 2.2 shows a bi-metallic tube which was used to study its axial crushing behavior.

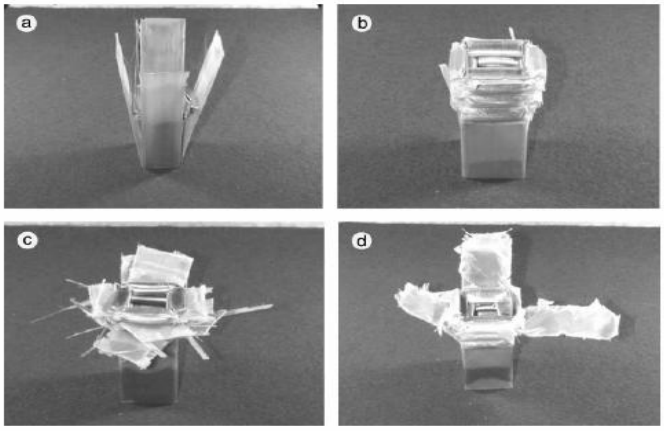

Figure 2.3 Bi-metallic tube of CFR on steel under axial crushing [11]

Mamalis et al. studied energy absorption characteristics of composites and their dependency on various factors like thicknesses of tubes, their fabrication characteristics, geometry and different volume ratios of composites.

As fabrication of composites is an important factor and it will increases the overall cost of structure, researchers have tried to come up with different materials that can be used as filler materials. Reid et al. [3] were amongst the first researchers who studied the behavior of sheet metal tubes filled with foaming material under axial crushing. Later studies are done on different types of foams like metallic and non-metallic foams and their effect as sandwiching material or filling material for different metallic tubes.

2.3 Effect of Foam Filling

Metallic foams were being used in automobile industry in different components to absorb the energy of an impact or in shielding devices to reduce the shock wave from a blast which might also have complex shapes. Aluminum, Nickel, Iron, Copper, Titanium and Platinum are some of the common metals which are used to prepare metallic foams. In automotive industry because of their light weight, aluminum foams become famous foams. Researchers like Giou et al. [12] conducted studies on aluminum foam materials to study their energy absorbing

capabilities when they are subjected to axial compressive loading. Figure 2.4 shows the tubular hat section which was crushed under an axial loading. It can be observed that by filling aluminum foam the number of foldings were increased.

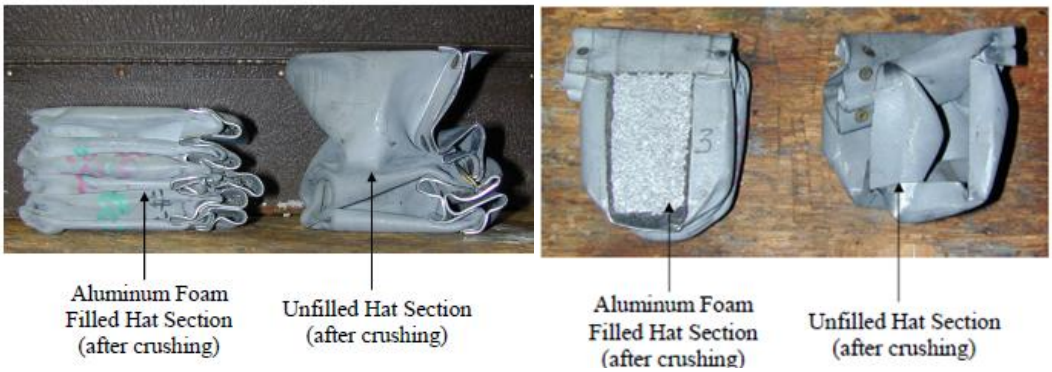

Figure 2.4 Crushing pattern hat section filled with aluminum foam [12]

In all of these cases, the foam may be subject to multi axial loads. In the design of sandwich panels, initial failure is critical and the engineer requires a criterion for initial failure. In the design of energy absorption devices, an understanding of the post-yield behavior as the foam locally densities are essential: In this case [12], a more complete constitutive equation describing the hardening behavior is required.

In Giou et al. [12] study a review was conducted on previous research on multi-axial failure criteria for cellular solids and described an experimental program was designed to measure the failure response of one open-cell and one closed-cell aluminum foam under uni-axial, bi-axial and tri-axial loading. The load verses displacement, energy absorbed verses displacement data from the experiments and the simulation results were plotted and compared in the Figure 2.5 with three proposed criteria for initial failures.

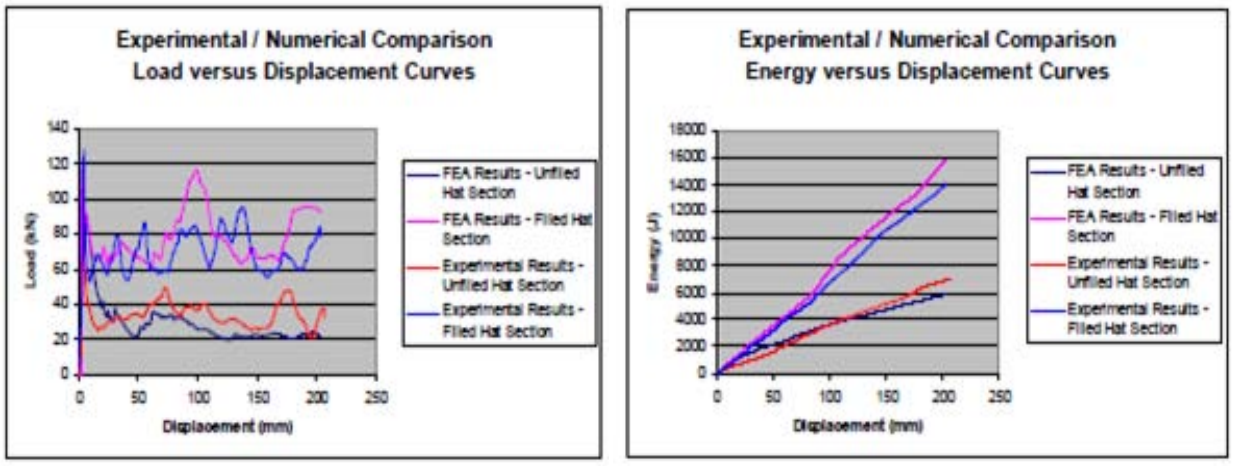

Figure 2.5 Energy absorbing capacity of aluminum foam [12]

Polystyrene and Poly-urethane foams are one of the commonly know low density foam materials which were being used as filling material in automotive and aerospace structures. Recent advancements shows that the properties of this type of foams can be improved by changing their material properties and hence researchers are continuously working to develop these materials as the fabrication, and weight to energy absorption characteristics are far better than any other foam materials [5].

In the research conducted by Mamalis et al., it was found that, filling steel tube with poly-urethane foam of 20 Kg/m^3 density; doubled its energy absorption capacity and almost doubled its specific energy absorption capacity [5]. Figure 2.5 shows load verses displacement curves from the study, here (a) represents the steel tube filled with poly-urethane foam material energy absorption characteristics and (b) indicates the energy absorption capacity of empty steel tube under quasi-static axial compression. They also proved an important analogy between the ratios of foam densities to the ratio of respective specific energy absorption. Figure shows the load verses displacement curves for empty and poly-urethane foam fill.

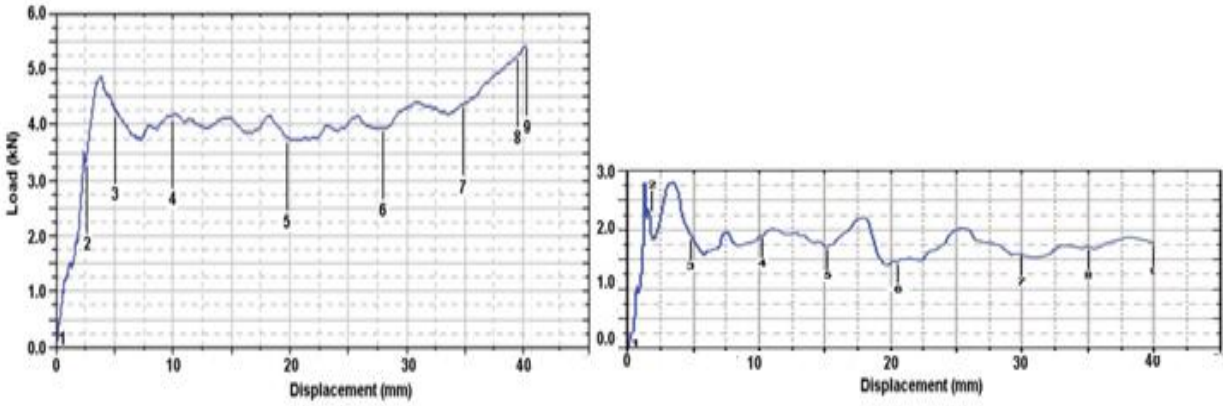

(a) (b)

Figure 2.6 (a) Foam filled tube (b) Empty thin walled steel tube [5]

From Mamalis et al. [5], study it was also observed that, the number of foldings that were formed during the axial compression of steel tube filled with Poly-urethane foam were almost thrice the number of folding which were produced by empty steel tube. In Figure 2.6 the effect of foam filling on folding pattern was clearly shown.

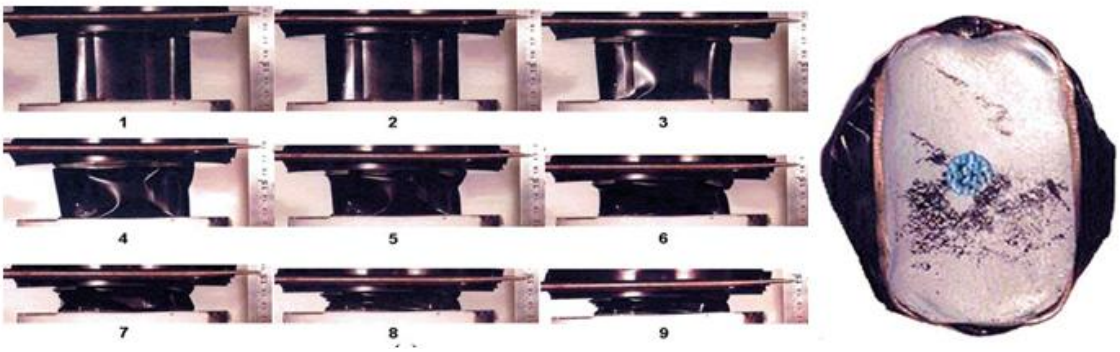

Figure 2.7 Effect of foam fill on folding patters of thin walled steel tubes [5]

CHAPTER 3

FOAM AS ENERGY ABSBORBING MATERIAL

3.1 Foam Materials

Foam is a substance that is formed when various gaseous bubbles are trapping in a liquid/solid [13]. Foam is in general an extremely composite system consisting of poly-disperse gas bubbles separated by draining films. The term foam may also be referred as something that is alike to such a phenomenon, such as quantum foam, polyurethane foam (foam rubber), XPS foam, polystyrene, phenolic, or many other manufactured foams [13]. The basic different types of foam materials are Liquid foams, Solid foams, Synthetic foams and integral skin foams

3.2 Different Foam Materials

Foam materials are usually classified depending on their area application. Engineering category of foams are typically solid foams which are lightweight cellular materials (metals or plastics). Again these foams are classified into two different categories based on their core structure as: Open cell foams and closed cell foams which are shown in Figure 3.1.

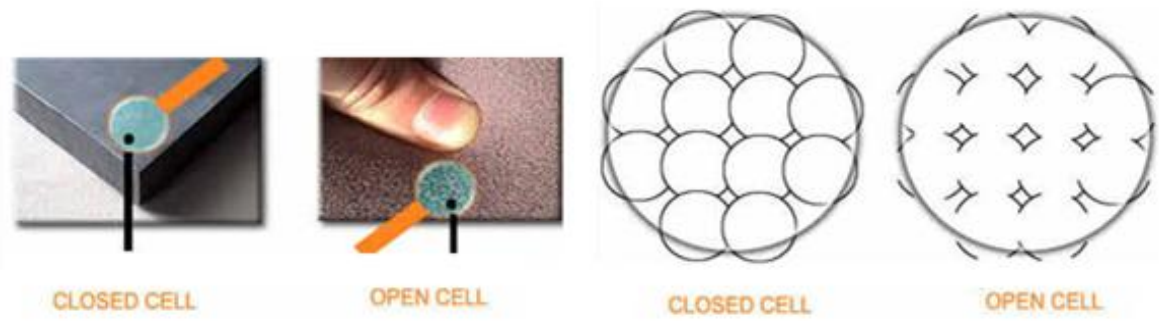

Figure 3.1 Open and closed cell structure of foams [13]

3.2.1 Open cell structured foams

Open cell foams are also called as reticulated foams which contain pores that are linked to each other and shaped as an interconnected network which is comparatively soft or the cell walls, or surfaces of the bubbles are broken and air fills all of the spaces in the material. This makes the foam soft and weak. Open cell foams are filled with surrounding materials which means either by gases or liquids. This makes them soft and the cushion depending on the surrounded material. Figure 3.2 shows a typical physical and magnified view of open cell structured foam material.

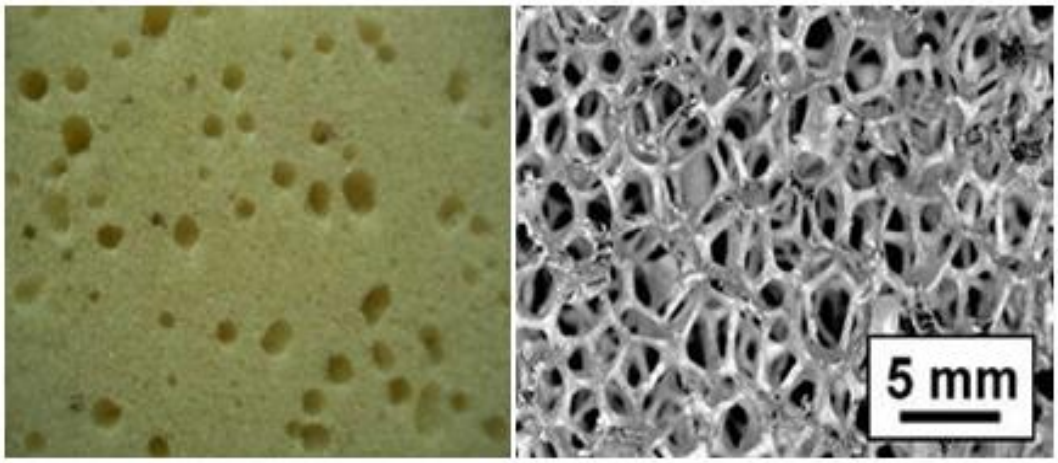

Figure 3.2 Physical and magnified view of open cell structured foams [13]

3.2.2 Closed cell structured foams

Contrasting to open cell foams, closed cell foams have no interconnected pores. Because this closed structured nature closed cell foams are superior compressive strength. However, closed cell foams are normally denser, and require more material to foam, hence automatically are much expensive to manufacture. Most of the time closed cells are filled with some specific gases to provide improved insulation for acoustics vibration applications. The main

characteristics of closed cell structure foams are that they have higher dimensional stability, little moisture absorption coefficients and superior strength compared to open cell structured foams. These type of closed cell foams are widely used as core material in sandwich structured composite materials. In Figure 3.3, a physical and a magnified view are shown. In this figure scale is used to explain its cell structure.

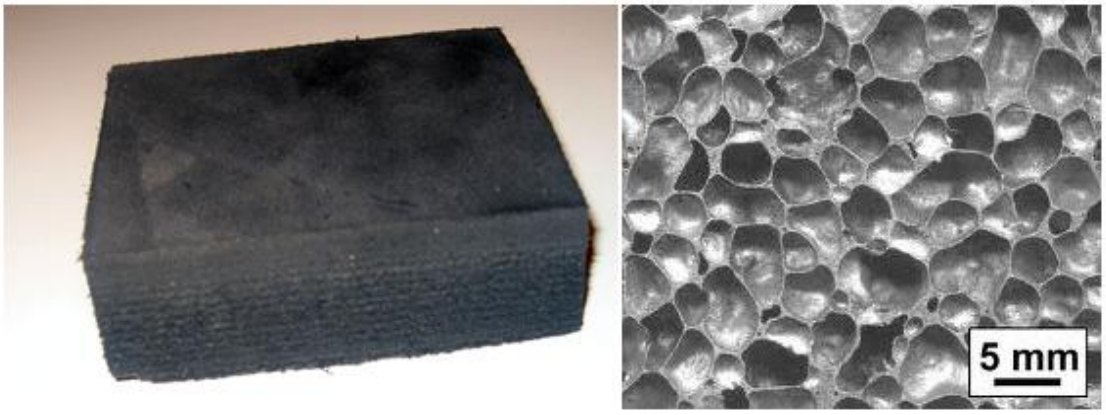

Figure 3.3 Physical and magnified view of closed cell structured foams [13]

From the early 20th century, different types of specially processed solid foams are made for different applications and uses. With their low density property these foams become famous and excellent use as thermal insulators, flotation devices. And their lightness and compressibility made them best fit in packing materials and padding material. Foam is almost about everywhere in the interiors of cars. The seats are made out of different types of foam. Synthetic cellular materials, polymeric and metallic foams, have been extensively used in energy-absorbing systems for decades. These materials are usually light in weight, stiff, and can absorb energy as well. In automobiles the door panels are often padded with thin sheets of foam unless they are made from molded plastic or some such material. Even the ceiling of the cars has foam

supporting the headliner material. The results obtained in energy-absorption tests indicate that polyurethane foam performs the best of all the materials tested; this made polyurethane foam use as a widespread impact safety material in vehicles.

3.3 Mechanical Properties of Foam Materials

The most common mechanical properties of foam materials depends on the base materials properties and these properties are Foam density (ρ_f), Foam modulus, and Crush strength. These properties are at least and mostly affected by the foam base material. Even though foams have distinct thermal, electrical conductivity, and acoustics properties, in this study the emphasis is made on their mechanical properties only.

3.3.1 Foam density

The actual density (ρ_a) of foam can be defined as the bulk density of the base material of the ligaments or struts (ρ_s) multiplied by the relative density (ρ_r) [13].

$$\rho_a = \rho_s \cdot \rho_r \tag{3.1}$$

Typically for metallic foams the density of actual foam is in the range of 2% to 15%; for carbon foams it is in the range of 3% to 4%; and for ceramic foams, it is in the range of 3% to 20%.

The majorities of foam manufacturers are providing material data including the relative density and this can be easily computed or confirmed by just weighing and measuring the part, and then divide the measured weight by pre-calculated weight by assuming the component as 100% solid material.

3.3.2 Foam modulus (E_f)

When a load is applied on foam structure, initially it will yield elastically. The slope of this initial linear portion of stress verses strain curve is defined as foam modulus (E_S) or as foam

stiffness. The young's modulus of a foam structure is a function of the solid material modulus and square of the foam structure relative density [13]. This can be written as an equation as,

$$E_f = E_s \cdot (\rho_r)^2 \tag{3.2}$$

where, E_f is the Young's modulus of the foam material

E_s is the Young's modulus of the strut

ρ_r is % relative density of foam (written in decimal form; i.e., 10% equal to 0.1)

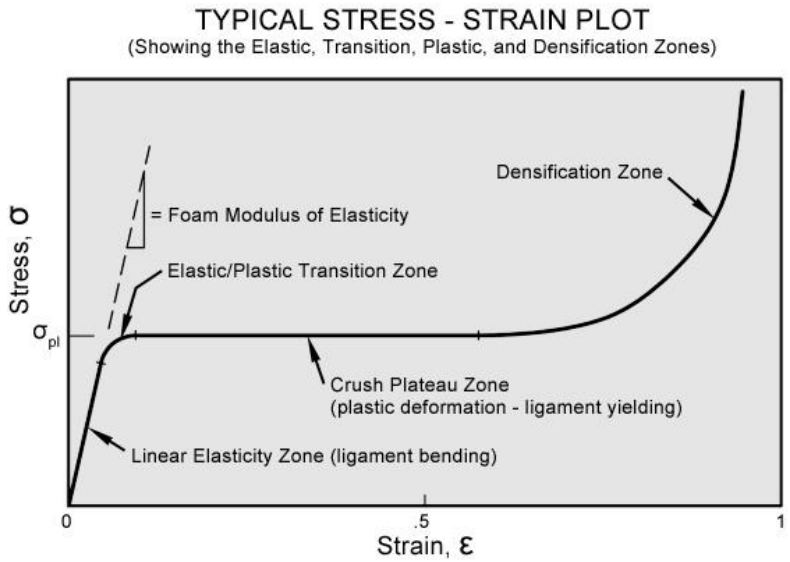

Figure 3.4 Deformation zones observed in foams [13]

Unlike foam density, which is a function of foam relative density, the modulus of the foam structure is a squared function of the relative density (ρ_r). This control of relative density in determining foam modulus over a wide range provides a dominant design tool.

3.3.3 Crush strength (σ_c)

After the foam's Young's modulus, the most useful property is the crush strength or plastic yield strength. Whenever a load is applied on a foam material structure, it will primarily

yield elastically in according with the young's modulus equation discussed above. However, the foam structure will start to buckle and collapse constantly at a moderately constant stress, at approximately 4% to 6% of strain depending on sample size. This steady collapse will proceed up to 50% to 70% of strain, depending upon the initial relative density of the foam. After this stage, the stress verses strain curve as shown in Figure 3.4 will start to rise as the compressed foam reaches the densification phase. The point in the stress verses strain curve where it transitions from the elastic to plastic deformation phase is defined as the crush strength of that particular foam. This is an important mechanical parameter as it is obviously important that the load should remain below that level strength for any structure which is designed to retain its shape below design load conditions. In contrast, the long, comparatively flat section of the curve in Figure 3.4 between the 4-6% transition state and 50-70% state represents a significant amount of plastic work. This unique characteristic of porous materials makes them very useful as energy absorbers where they absorb the kinetic energy of an impacting mass in a controlled manner, and this controlled load carrying capacity is represented by its crush strength.

For any given rigid and collapsible foam structure the crush strength (σ_c) is an important design characteristic, and it is simply defined by the foam modulus by fallowing equation [13]:

$$\sigma_c = 0.58 \cdot \sigma_y \cdot (\rho_r)^{3/2} \tag{3.3}$$

where, σ_c is the stress at which continuous plastic collapse starts

0.58 is the co-efficient from actual compression data

σ_y is the tensile yield stress of the foam struts

ρ_r is the % relative density (written in decimal form, i.e., 10% equal to 0.1)

There are some other foam characteristics; the ones presented above can deal with primary mechanical design concepts. The other main important parameters of the foam are: foam material, pore size, and relative density, which are independent variables, and thus provide a three-dimensional design space of equal importance and thus making any of the foam characteristics as functions of any of these independent variables.

3.4 Effect of Nano Particles on Foam Properties

As discussed earlier the properties of the foam materials depends on the base material and the composition of the base and the additional materials which are used to prepare the foaming material. Researchers, engineers are investigating and conducting research to develop foam materials which not only light in weight but posses superior mechanical, thermal properties. Saha et al. conducted research on foam materials [7]. They infused different nano particles into polyurethane foam and studied there effect on the mechanical, thermal and chemical properties of the foams. The different types of the nano particles used were spherical TiO_2, platelet nano-clay, and rod shaped carbon nano-fibers (CNFs).

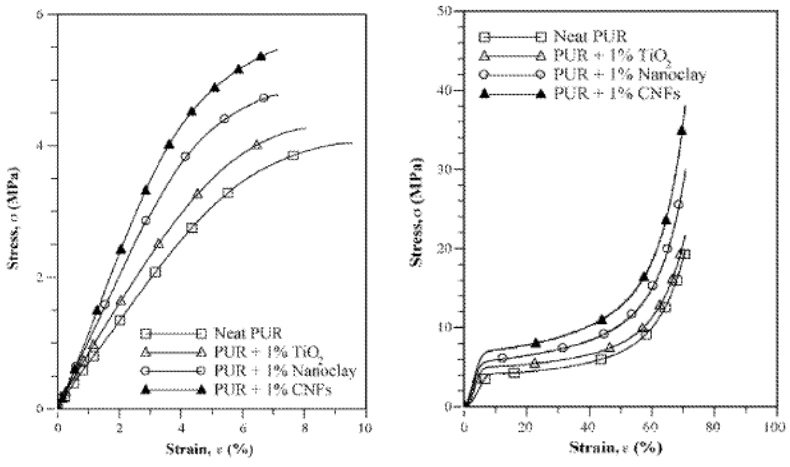

Figure 3.5 Mechanical properties of carbon nano foams [11]

In Saha's study, the 1 % weight of nano particles were added to poly-urethane foam and the resultant nano-phased foams were tested in tension, compression and flexural test conditions. The results showed that the addition of nano particles improved the mechanical properties of that nano phased foam material by a significant amount [7].

Figure 3.5 gives the details of compression test results when poly urethane foam infused with different nano particles. Test samples are tested till the compression reaches 70% of densification and found that poly-urethane foam infused with carbon nano tube particles shows much better results than any. Table 3.1 from the Saha's study shows that there is significant amount of increase in compressive modulus, compressive strength in poly-urethane when nano particles are infused into it. When different nano particles are compared, it is found that the addition of carbon nano tube particles gives lot better results and the gain in compressive strength and compressive modulus was 56.8% and 40.0% respectively [7].

Table 3.1 Tabulated results on different nano foam materials [7]

Material	Sample No.	Compressive Modulus (MPa)			Compressive strength (MPa)		
		Data	Average +/- SD	Gain (%)	Data	Average +/- S.D	Gain (%)
Neat	1	133.6	130.2 5.4	-	4	3.7 0.3	-
	2	124			3.3		
	3	133			3.8		
1 wt % TiO2	1	137.9	146.3 7.3	12.4	4.1	4.3 0.2	16.2
	2	151.3			4.5		
	3	149.7			4.3		
1 wt % Nano Clay	1	164.8	156.7 7.2	20.4	5.1	5.1 0.1	37.8
	2	154			5.2		
	3	151.3			5.2		
1 wt % CNFs	1	180.5	182.4 2.3	40.1	5.8	5.8 0.1	56.8
	2	181.8			5.8		
	3	184.9			5.7		

CHAPTER 4
COMPRESSION TEST OF CNF FOAM

4.1 Introduction

Foams are basically subjected to compression loading conditions; as foams are weak in tension, shear and hence they are rarely subjected to deformations in this type of loading conditions. In this study, five different types of foams are subjected to same range of compression at similar rate of loading and testing conditions.

4.2 Specimen Preparation

In this experiment, open cell poly-urethane foam of density 27 kg/m^3 was used as the base material. Specimens of poly-urethane foam and poly-urethane foam infused with carbon nano fibers (CNF) test specimen were prepared. The preparation of foam material was accomplished in three different stages. First, the amount of material that is needed for the formation foam are calculated and weighed carefully. In this study 1% to 4% weight of carbon nano tubes are added into the solution of foaming agents to form four different specimens.

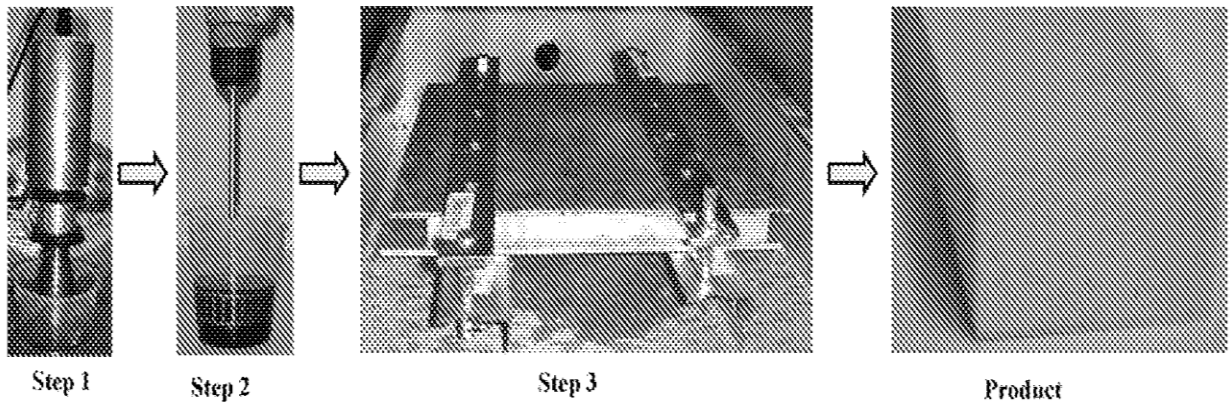

Figure 4.1 Manufacturing steps for nano poly-urethane foam [7]

Second stage, these pre- calculated amounts were than mixed properly. This mixing process was the crucial part of foam preparation because the quality (homogeneity) of foam produced is entirely depends on this fixing as this controls the homogeneity of the resultant foam. Figure 4.1 shows the details of preparation of foam materials.

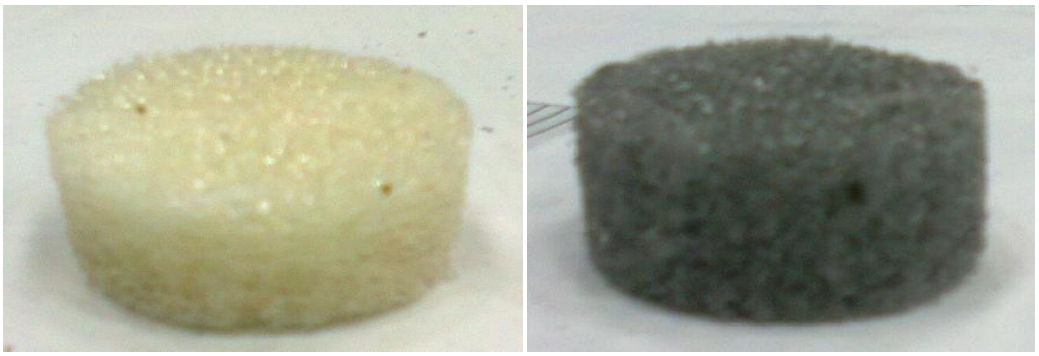

(a) (b)

Figure 4.2 (a) Poly-urethane foam specimen, (b) CNF foam specimen

After the preparation the foam materials, foams were cut into required test specimens shape and size. These test specimens were of right cylindrical shape with 12.5 mm radius, 12.5 mm thickness. Figure 4.2 (a) and (b) gives the details of neat poly-urethane and nano phased poly-urethane foam (CNF) material test specimen which are used in this compression test. In this study the specimen effects, shape effects are neglected and minimum corrections like smoothing and toe corrections are included.

4.3 Test Set-Up

Once the specimen sample preparation was done, the specimens were moved to test site to arrange the specimen to conduct compression/crush test. To carry out this compression test exact or appropriate load cells are selected and are fixed into the MTS testing machine. The specimens were carefully placed in the middle of the right cylindrical base plate to minimize the shape effects during the test. Loading rate is set to the required rate and a sample test was carried

out to make sure the test method and the results obtained were appropriate. Figure 4.3 shows the compression test set up used in this study.

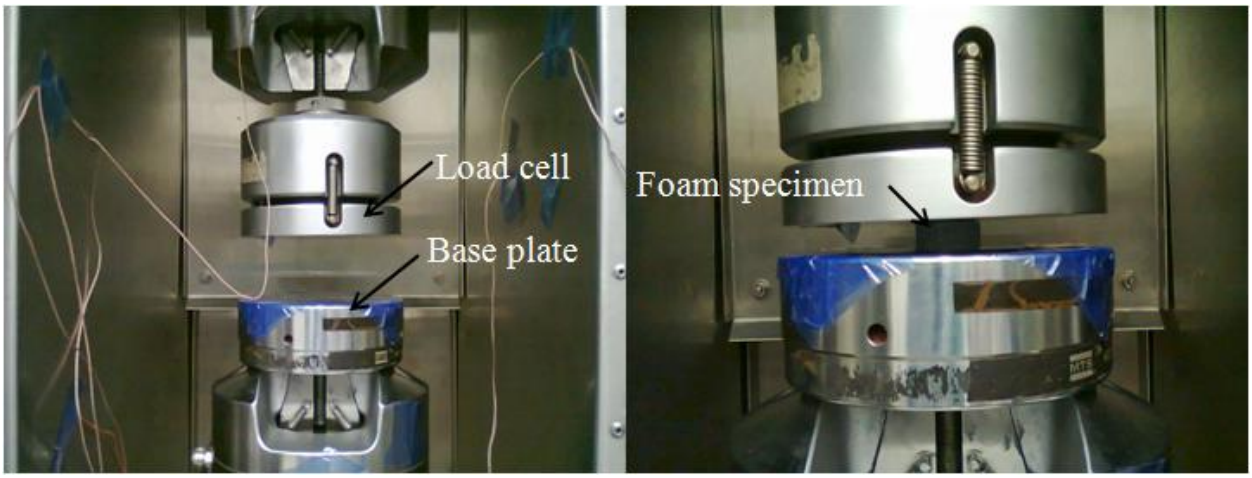

Figure 4.3 Test set up used for carbon nano foam compression test

4.4 Results and Discussions

Static compression/crush tests were conducted on foam specimens to determine whether there is any enhancement in the load carrying capacity of poly-urethane foam infused with carbon nano tubes and to quantify the improvements in energy absorption prior to ultimate failure. The carbon nano tube infused foam specimens were tested till the specimens undergo 70% - 75% compression with a cross head speed of 0.127 mm/s (i.e., 0.05 in/s) by using a servo-hydraulic MTS testing system. Specimen data is recorded by using TestWare-SX, a data acquisition system. The data for load verses crosshead displacement was recorded. Test specimens were of same nominal height and width in static testing. Data obtained from the test was reduced by taking the average loads as required to visualize and remove noises from the test data. The average loads were then used to plot load verses displacement and stress verses strain plots. A common behavior plots are used to characterize the effects of carbon nano fiber addition

into poly-urethane foam. Energy absorption capacities of each type of foam material tested were calculated and compared with (neat) poly-urethane foam

Table 4.1 Compression results of nano phased materials (70% densification)

Specimen	***Mean load (lbs)***	***Energy (lbf)***	***% Increase in energy absorption***
FOAM	21.0	7.7	-
CNF 1%	26.8	10.6	37.4
CNF 2%	26.4	10.1	23.2
CNF 3 %	32.1	12.4	46.0
CNF 4%	20.0	8.1	3.1

The test results are summarized and tabulated in the Table 4.1. Specimen data for test are filtered by using statistical tool in Microsoft Excel, and the filtered data was plotted as graphs. Figure 4.4 shows the details of the reduced data, where different foam samples are represented with different solid color and each sample of specific foam data was shown in same color, but using dotted lines (two specimens for each type of foam). From the results it is clear that the addition or infusion of carbon nano fiber particles into poly-urethane foam will certainly increase the load carrying capacity of that nano phased poly-urethane foam.

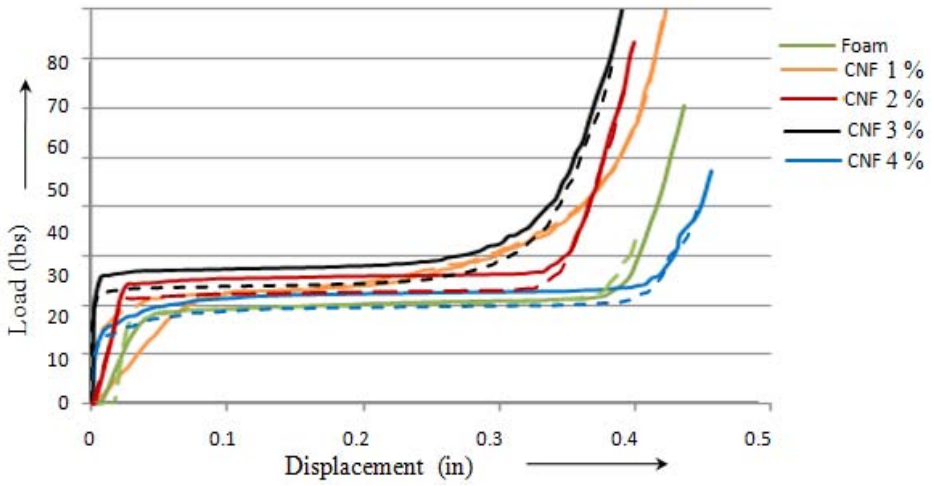

Figure 4.4 Compression test results

. From all the nano phased foam samples tested, poly-urethane foam infused with 3 % weight of carbon nano fibers(CNF) showed highest load carrying capacity (12.4 lbf) and 4 % weight of CNF foam being the lowest (8.1 lbf). From the results, it is evident that the addition of carbon nano tube particles ranging from 1 % to 2 % weight of CNF would definitely increase the mechanical properties of poly-urethane foam [7]. When energy absorption characteristics of each nano-phased poly-urethane were compared, it was found that, as the percentage of carbon nano fibers increased from 1 % to 4 % weight, the energy absorption capacity of that nano phased poly-urethane was increased until 3% weight and a very little or negligible amount of increase was observed in 4 % weight nano phased poly-urethane foam samples. From Figure 4.5, one can observe the phenomenon that, addition of CNF to poly-urethane foam increased its energy absorption capability by 46 %, when compared to neat poly-urethane foam.

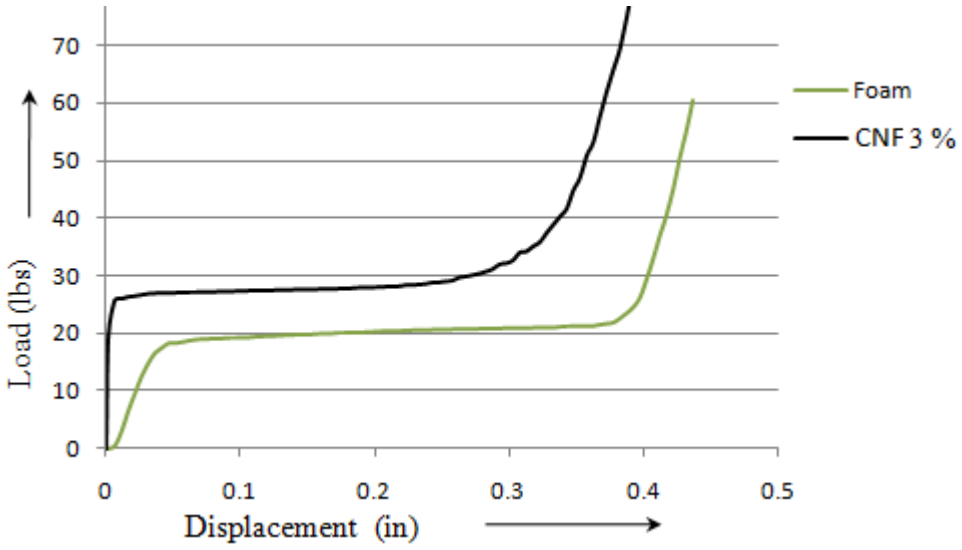

Figure 4.5 Comparison of foam vs CNF foam compression test results

.

CHAPTER 5

FINITE ELEMENT MODELING OF CRASHWORTHY TUBE

5.1 Introduction

The finite element methods are used to solve complex elasticity and structural problems in civil and aeronautical engineering. These methods are originally introduced by Hrennikoff and Courant [14] in 1941-42 for solving second order elliptical differential equations arised from torsion of cylinder. Development of these methods again started after 1947 by Zienkiewicz, Rayleigh, Ritz and Galerkin [14]. As the usage of computers in solving mathematical and physical problems got popular, cheaper and less time consuming, researchers started developing codes which utilizes finite element methods to solve structural problems using computers. In 1965, NASA has developed Nastran as the first software which utilizes these methods.

Finite element analysis of structures or any mechanical system is basically performed in three stages: pre-processing, analysis and post-processing. In pre-processing, creation of geometry is the first step than meshing of this created geometry is second and in final step materials properties and boundary conditions are specified. Once this procedure has completed an analysis code is used to perform analysis to generate the results. These generated results are then visualized in a post processor. In this study the Altair Hypermesh is used as pre-processing tool, Ls-Dyna as analysis code and Ls-Prepost is used as both pre and post-processing tool.

Ls-Dyna is an advanced general-purpose multi-physics highly nonlinear transient dynamic finite element analysis simulation software package tool developed by the Livermore Software Technology Corporation (LSTC). This software package is a multi-functional tool which uses implicit time integration method for static and explicit time integration method to perform nonlinear dynamic finite element analysis. While LSTC is continuously adding more

and more capabilities to Ls-Dyna to compute many complex and real world problems and is being used by the automotive, aerospace, construction, military, manufacturing and bioengineering industries. This code consists of a wide-range library which includes membrane, thin / thick shells and solid formulation.

An important feature of this software tool is its capabilities to produce fully automatic definition of contact areas. The user interface is intuitive and easy to use. These features allow the user to utilize Ls-Dyna for a wide variety of applications. Few of the main applications of this tool is in automobile industry to study crashworthiness behavior of various structures, manufacturing industry to analyze metal forming, and in electronic industry to test and analyze components drop test.

5.2 Classifications of Loads

In engineering applications classifications of loading will be done with respect to the rate of loading or rising time of the mechanical system and depending on this there are four types of loadings: Static load, fatigue load, high speed or rapid load and impact or shock load. Figure 5.1 shows a typical loading curve; where on a system a load (P) was applied. Before the load reaches its maximum value (P_{max}), the application was assumed to be linear and the time taken by the load to reach its maximum value will distinguish the type of loading applied on that system.

5.2.1 Static load

Static load is defined as the load where the rise time of the load should be at least three times greater than the fundamental time period (T_n) of the mechanical system [14]. This type of loading remains constant with respect to time. In this type of systems the analysis is carried out to develop stress verses strain or load verses displacement to find static material properties.

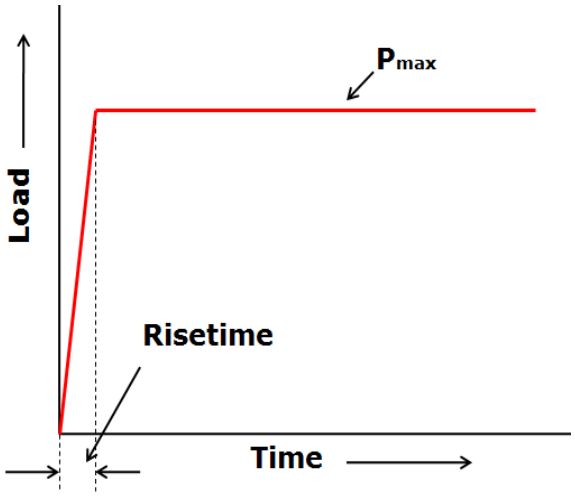

Figure 5.1 A typical load verses time curve

5.2.2 Fatigue load

It is similar to static loading but the only difference here is that the load varies with time and this variation of load with respect to time remains constant. And as in case of static rise time of the load is three times the fundamental period (T_n).

5.2.3 High speed or rapid load

In this method, the rise time of loading ranges between 1.5 to 3 times of fundamental time period (T_n) of the mechanical system and this type of loading widely used in vibration analysis method of stress and displacement study.

5.2.4 Shock or impact load

In this type of loading, the rise time of loading is less than 0.5 times the fundamental period (T_n) of the mechanical system [14]. Impact loading is one of the most expensive types of experimental study as the equipment and prototypes requited to test the specimens are expensive. This form of testing is destructive type and any mistake during the test will result in inappropriate data.

Because of these drawbacks finite element analysis has been considered to be the most alternative solution method to mimic the actual experimental impact tests. In case of finite element analysis any flaws can be easily corrected and they hardly affect the final results and this gives the flexibility to change various process/design parameters of the test with no any additional expense.

5.3 Modeling Details of Present Study

In this present study finite element modeling is done by using Hypermesh. Components which are modeled in this study are foam model, a steel tube model, and steel tube filled with foam material. Each model is modeled by considering all boundary conditions. Discussion on each model is as fallows.

5.3.1 Finite element modeling of tube structure

Modeling of thin walled steel tube is done by using Hypermesh. In this present analysis appropriate element size is selected for the thin walled steel tube and foam material and at the same time quality of the mesh is checked. The dimensions of the rectangular steel tube are 93 mm × 49 mm × 54 mm and with 0.3 mm thickness. All four corners of rectangular tubes are chamfered with corner radius 15 mm, all the modeling details are tabulated in the Table 5.1. This model is used to check the behavior of material card with respect to the experimental results

Table 5.1 FE model details of tube specimen

Element Length for tube model	2 mm
Number of Nodes in tube model	11073
Number of Elements in tube model	1296

The dimensions of the carbon nano foam material are calculated by considering the thickness of the steel tube material and the element size of the foam is considered to be twice the element size of the steel tube [15]. Figure 5.2 represents the models which are utilized in this analysis

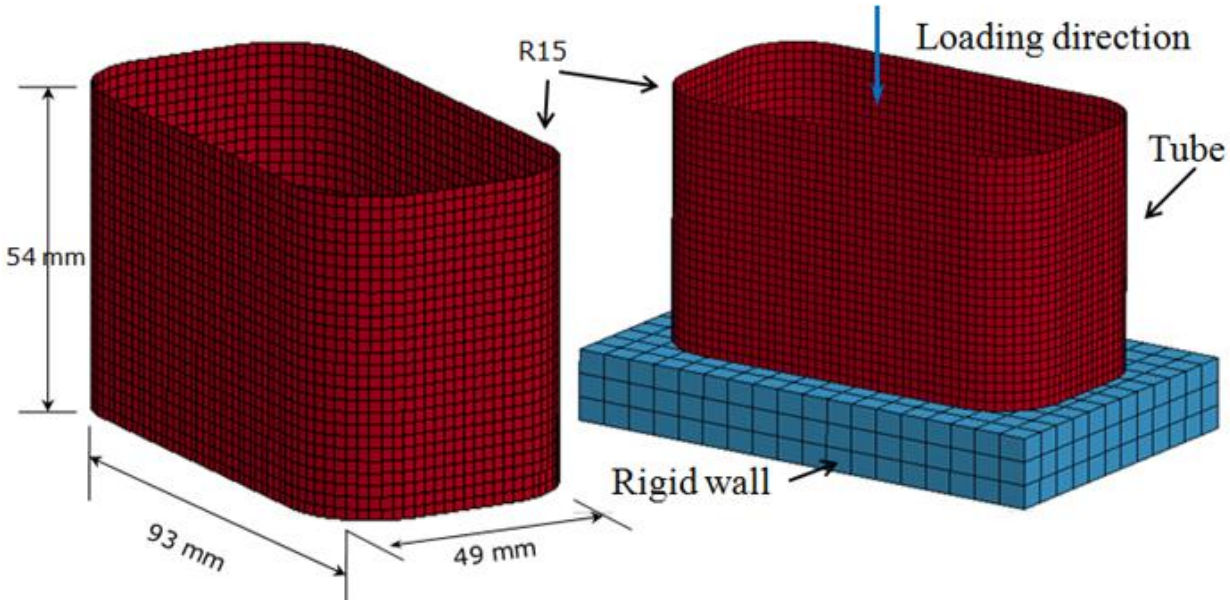

Figure 5.2 FE models of steel tube with loading conditions

Figure 5.3 gives the details of the carbon nano foam model which is utilized to perform its material validation. The dimensions of the carbon nano foam are selected as 25 mm × 25 mm × 12 mm as of the test conditions. In Table 5.2, the details of element size, number of elements are discussed and in the Figure 5.3 FE model utilized for foam material validation with its boundary conditions are represented.

Table 5.2 FE model details of foam material model

Element Length for foam model	4 mm
Number of Nodes in foam model	6878
Number of Elements in foam model	6268

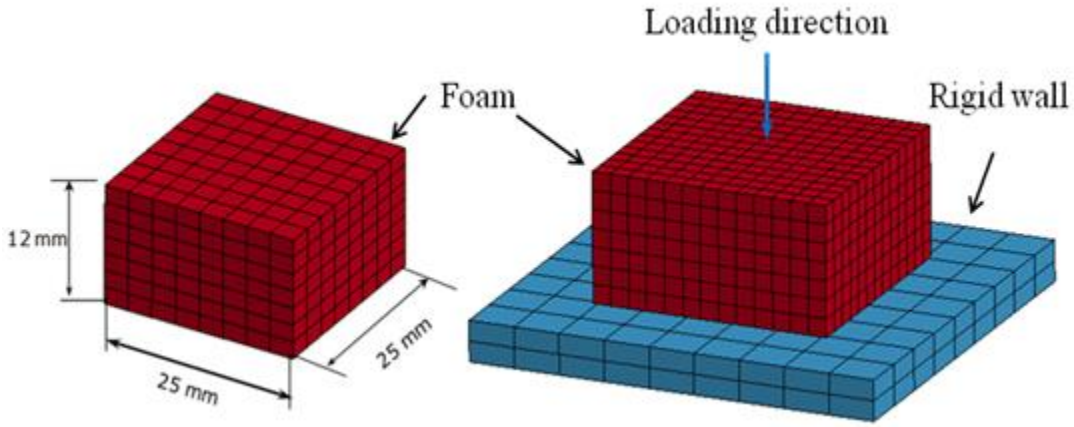

Figure 5.3 FE model used for CNF material validation

In this simulation, empty steel tube, carbon nano foam and steel tube with carbon nano foam materials are compressed by a rigid wall. The bottom rigid wall is fixed in three directions of translation and rotations. The upper rigid body is allowed to translate in only z-axis direction which in this case corresponds to the moving direction of the impact mass. The dimensions of these two rigid bodies are chosen such a way that, they will be in contact with tube in every stage of the simulation and as the energy absorption hardly effected by impact mass [7, 5].

5.3.2 Material modeling

Steel and carbon nano foams are the two materials which are used in this analysis. As rectangular steel tubes are made of steel so, MAT_24 (*MAT_PIECEWISE_LINEAR_PLASTICITY) material card is used to mimic its properties. MAT_024 is of the most commonly, efficiently used material card [14]. This card is based on piecewise linear isotropic plasticity material type which utilizes von-mises flow rule. In this material model an arbitrary stress and strains can be defined by using the define curve option. The materials properties of the steel tube are obtained from tension tests performed on the specimen of the tube are tabulated in Table 5.3.

Table 5.3 Material properties of steel tube

Mass Density	7.8 g/cc
Young's Modulus	207 GPa
Poison's Ratio	0.3
Yield Stress	0.270 GPa

Carbon nano foam materials are crushable foams with very less recovery, unlike foam materials which are used in most of the automotive and aerospace seating systems. There are different material models available in Ls-Dyna code to represent foam materials. Common material models used by researchers are MAT_LOW_DENSITY_FOAM (MAT_053), MAT_CRUSHABLE_FOAM (MAT_063), and MAT_MODIFIED_CRUSHABLE_FOAM. As carbon nano foams are rigid foams and in this study the strain hardening and strain rate effects of the material are not considered, and hence MAT_CRUSHABLE_FOAM material card is used to capture the CNF foam behavior. In Table 5.4, CNF material properties are tabulated.

Table 5.4 Material properties of carbon nano foam

Mass Density	242. Kg/m^3
Compression Modulus	182.4 MPa
Compression Strength	5.8 MPa
Tensile Modulus	255 MPa
Poisson's Ratio	0.0
Tensile Strength	4.4 MPa
Flexural Modulus	207.3 MPa
Flexural Strength	6.7 MPa

In this material model, arbitrary yield stress versus volumetric strain values are defined using a define curve. The volumetric strain is defined in terms of the relative volume V [14],

As $$\gamma = 1 - V \tag{5.1}$$

where, γ is the volumetric strain and

V is the relative volume

but as lateral deformation of foam is negligible, Poisson ratio is taken as zero. In this case as Poisson ratio is zero, the volumetric strain can be replaced by linear strain obtained from the experiment and this can be used in the curve which is utilized to define the material model. The Figure 5.4 shows the define curve generated by using the experimental data. Material card MAT_RIGID (MAT_20) was assigned to the two rigid heads, which are practically not deformed during a crush test. Yet, as necessary by the Ls-Dyna code, the basic material properties (mass density, Young's modulus and Poisson ratio) corresponding to mild steel is assigned as input.

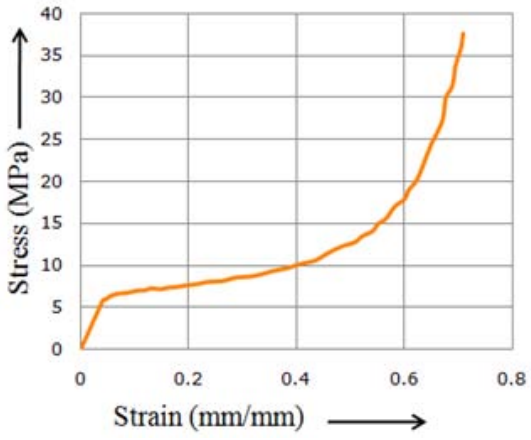

Figure 5.4 CNF numerical model

5.3.3 Failure criteria

Tubes are basically modeled using shell elements or thick shell elements based on their thickness. In this analysis 0.3 mm thick mild steel is modeled using 4-noded quadrilateral shell elements with five through-the-thickness integration points and based on Belytschko-Lin-Tsay shell elements which present macro-scopic distortion in improved manner [5, 12, 15]. Belytschko-Lin-Tsay element formulations are used because of its computational efficiency when compared with Hughes-Liu shell element models and this model is based on the assumptions like combined co-rotational and velocity-strain formulation which simplifies the given mathematical equations. Co-rotational portion of the formulation avoids the complexities of nonlinear mechanics by embedding a co-ordinate system in the element and the velocity strain, which is nothing but rate of deformation in the formulation facilitates the constitutive evaluation, because the conjugate stress is similar to Cauchy stress.

5.4.4 Contact modeling

In any finite element analysis, contact algorithms are the most important factors or conditions which are carefully selected. The entire analysis results depend on these contact parameters. Generally in any analysis there are basically two types of interactions occur. First, contact between any two bodies and the next contact with a body itself. In this analysis there are five contacts that occur between rigid-walls, foam and a self contact of steel tube during the compression. Depending on the type of contact between two or more parts interactions CONTACT_AUTOMATIC_SURFACE_TO_SURFACE and CONTACT_AUTOMATIC_ SINGLE_SURFACE algorithms are used in this analysis. Self contact was defined for simulating the behavior of the collapsible steel tube elements to itself which uses nodal normal projections to eliminate penetration of the elements into adjacent elements. SOFT artificially

reduces the strength of the row of elements immediately ahead of the active crush front. In this analysis SOFT has taken as 0.5 for better stability of the simulation. The dynamic and static coefficient of friction between steel tube and foam interfaces was assumed to be 0.25 and 0.3 respectively [14].

The load was applied using BOUNDARY_PRISCRIBED_MOTION card and cosine curve was applied to eliminate the sudden interaction between the slave and master bodies. In any analysis the initial loading rate will effects entire results, sometimes causes instabilities or gives rigid responses in the simulations. To avoid such scenarios, cosine curve is utilized, which not only reduces the initial stiffness of the simulation but also reduces the ramp loading to a smooth loading till the load reaches its maximum value. Figure 5.5 shows details of a cosine curve, where the velocity is applied very slowly which eliminate initial ramping effect.

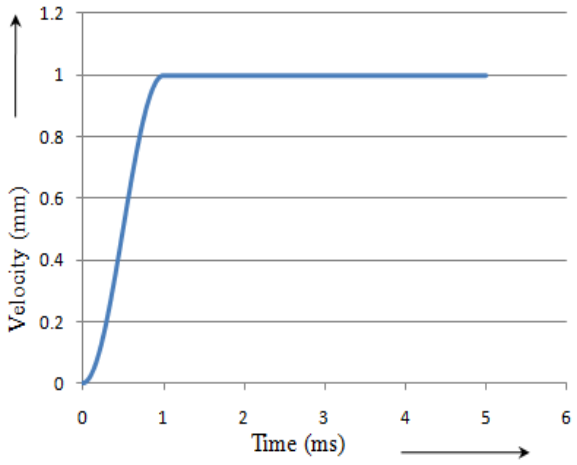

Figure 5.5 Typical cosine curve used in this study

CHAPTER 6

VALIDATIONS AND APPLICATIONS

6.1 Validation of Material Models

In this present analysis two different material models are validated against their experimental results. First, steel material is validated by simulating it for quasi-static uni-axial compression test. Second, carbon nano foam material is validated under similar conditions as of the experiment. Ls-Dyna code is utilized to simulate this experimental work done by Mamalis [5] and Saha [7]. After performing each analysis the ratios of energy are compared to make sure their values are within the reasonable limits.

6.1.1 Validation of steel material

Mamalis [5] had conducted experiments on thin walled steel tube with and without foam filling and utilized Ls-Dyna FE code to simulate these experiments to study the crush behavior and energy absorption characteristics under quasi-static axial loading conditions. The quasi-static axial compression tests were conducted utilizing Instron testing machine of 10 kN loading capacity at a crosshead speed of 20 mm/min which is of $6.1 \times 10^{-3-S}$ compression strain rate. The tabular tube's material is mild steel with 0.3 mm thickness and Young's modulus of $E = 21 \times 10^4$ MPa, yield stress σ_Y = 240 MPa, ultimate stress σ_U = 370 MPa. To simulate the experiment conducted by Mamalis, thin walled steel tube is modeled with similar geometric, material, and boundary conditions. To decrease the computational time, in this simulation the cross head speed in increased to 1 mm/s [5].

The results of the simulation are compared with the experimental results to check the accuracy of the material model. And it is found that the load verses displacement curve obtained from simulation results is very close to the curve obtained from experimental test results. Figure

6.1 shows the load verses displacement diagram was plotted as load in y direction and axial crushing displacement in x axia direction. In terms of mode of deformation, load deflection curves, and amount of energy absorbed, the theoretical results obtained by Ls-Dyna code and the observations made from experimental results are in good agreement. The divergence of 4.8 % increase in mean post crushing force in simulation compared to experiment was observed.

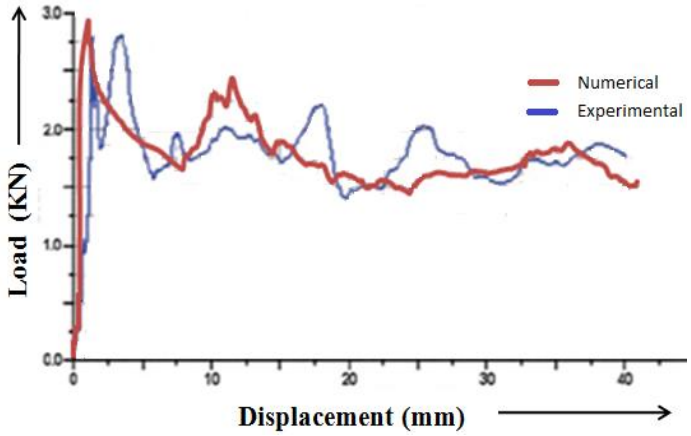

Figure 6.1 Steel tube load – displacement curve

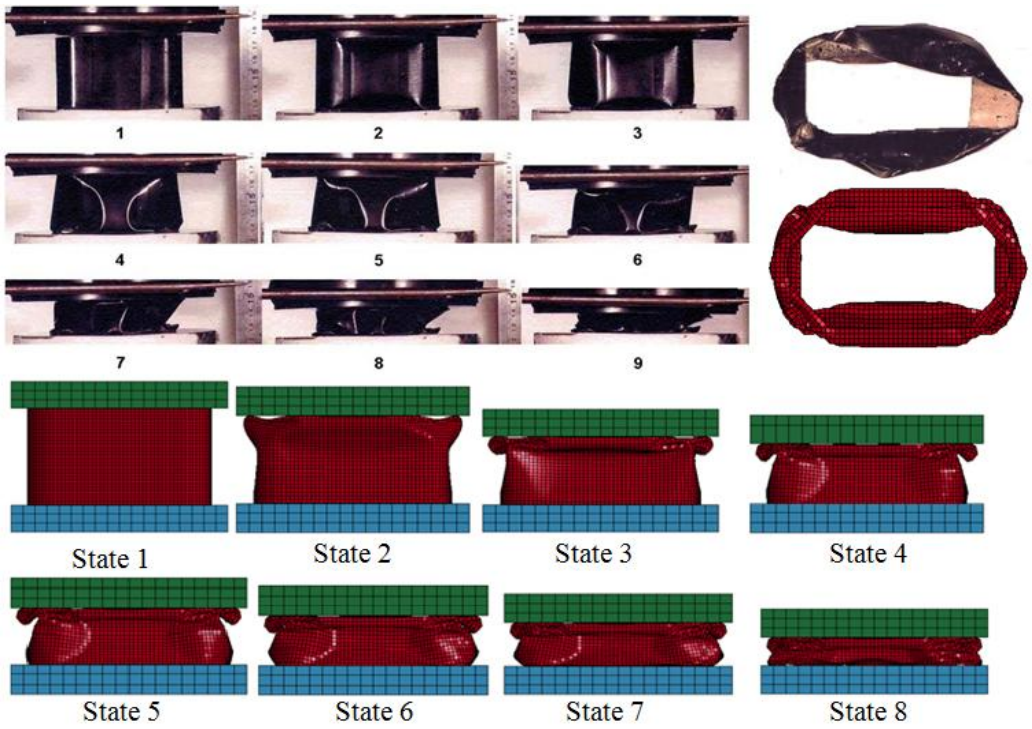

Figure 6.2 Crushing pattern of steel tube at different stages [5]

In Figure 6.2, the crush patterns of steel tube from the experiment at different states are compared with the crushing pattern obtained at different time step of the simulation. It is observed that in the experiment, the steel tube foldings are improper (out of plane buckling) which leads to less energy absorption when compared to the simulation.

6.1.2 Validation of carbon nano foam material

Saha et al [11] performed quasi-static axial compression tests on carbon nano poly-urethane foam of cube specimen with 25.4 mm x 25.4 mm x 12.7 mm dimensions using a servo-hydraulic MTS testing system. Figure 6.3 shows the details of the FE and material model of CNF foam. Tests are performed according to ASTM C365-00 at crossheads speed of 0.127 mm/s [9]. The compression load is applied till load reaches 70% densification of the specimen.

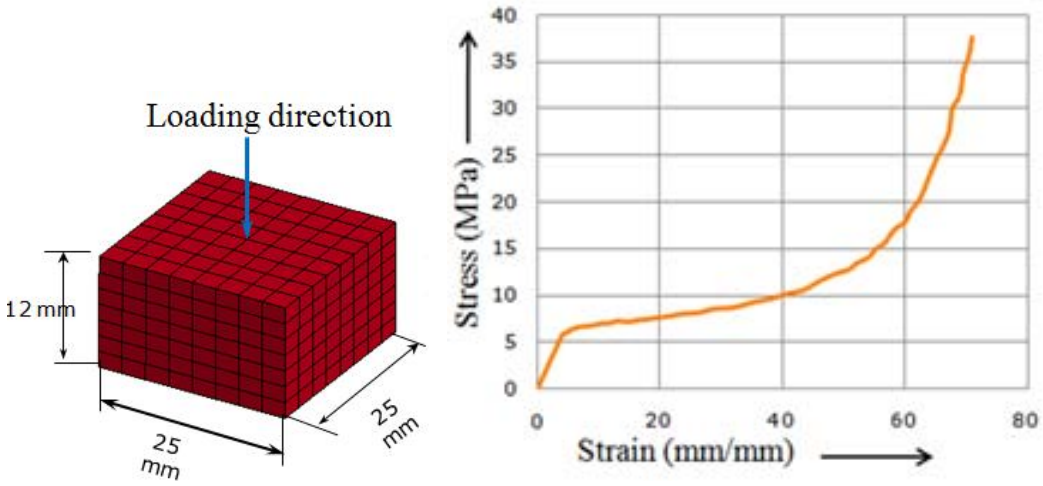

Figure 6.3 FE and material model of CNF

The material properties results obtained from the simulation are compared with the experiment and found that the numerical model utilized for this study behaves very close to the stress- strain curves of CNF compression test data, with 5 % divergence, as shown in Figure 6.4.

In Figure 6.5 the behavior of CNF foam in different stages of compression is clearly observed. As defined in the material model, CNF FE foam model did not strains in the lateral directions.

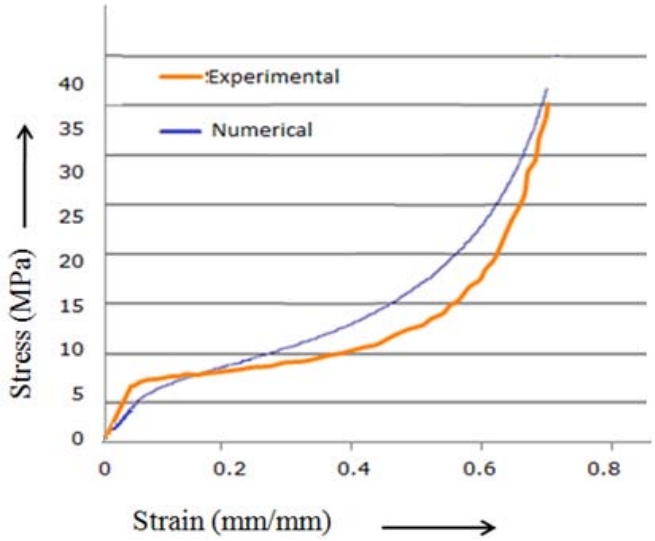

Figure 6.4 Stress verses strain plot of CNF material

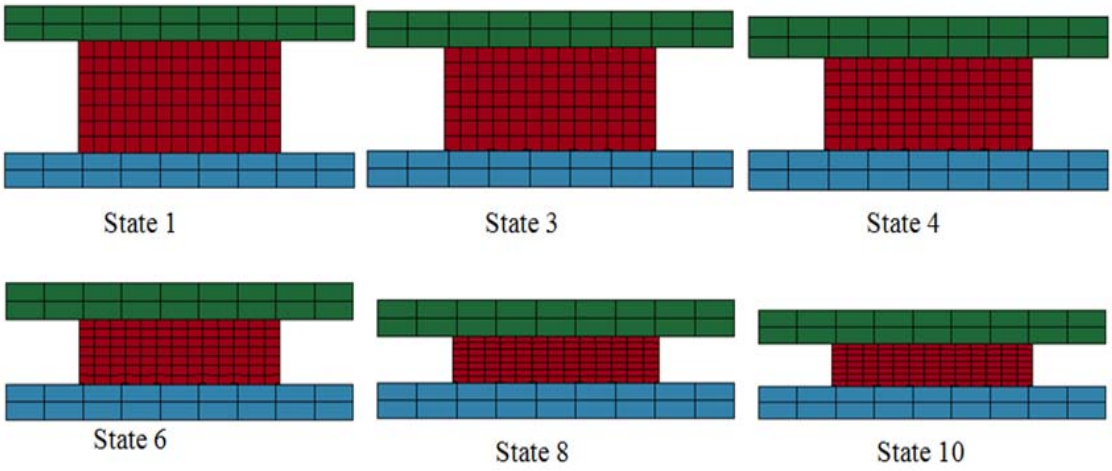

Figure 6.5 Crushing patter of CNF at different states

6.2 Application of Carbon Nano Foam

As suggested by previous studies foam materials are being used as padding or core materials automotive structures to improve their crashworthiness. In this present work, analysis is conducted to study the behavior of carbon nano foam when it is used as filler material in thin

walled steel tubes. First, steel tube of dimensions similar to the test conducted by Mamalis [5] is filled with carbon nano foam and the resultant structure is crushed under quasi-static conditions similar to the physical test. These results are then compared to the results obtained by the empty tube and steel tube which is filled by poly-urethane foam. Second, carbon nano foam is introduced as filler material into the bumper of dodge caravan vehicle model. This modified model will be used to study the behavior of vehicle under frontal impact at different speeds.

6.2.1 Rectangular thin walled steel tube filled with carbon nano foam

In this case rectangular steel tube with of dimensions 49 mm x 49 mm x 54 mm with a chamfer of 15 mm radius and 0.3mm thickness is modeled and this tube is filled with carbon nano foam of 48.85 mm x 93.85 mm x 53.85 mm dimensions. Figure 6.6 shows the details of dimensions, boundary conditions of thin walled tube which is filled carbon nano foam. The resultant structure is than crushed under at a cross head speed of 1 m/s.

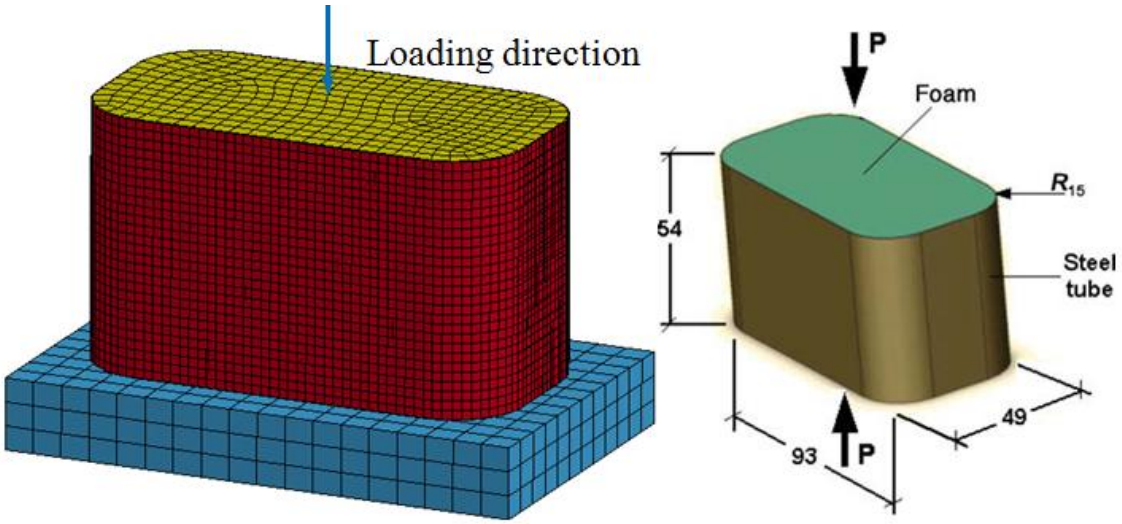

Figure 6.6 Carbon nano foam filled structure

From the analysis, it is found that the energy absorption capacity of empty thin walled steel tube increase from 71.4 J to 181.0 J, when it was filled with CNF foam. This increase in

energy absorption is much significant amount and 150 % more when compared to empty steel tube. Figure 6.7 shows the load verses displacement diagram representing amount energy absorbed by the empty thin walled steel tube to the CNF foam filled thin walled steel tube. It is observed that the stiffness of the resultant structure is increasing as the crushing distance increased.

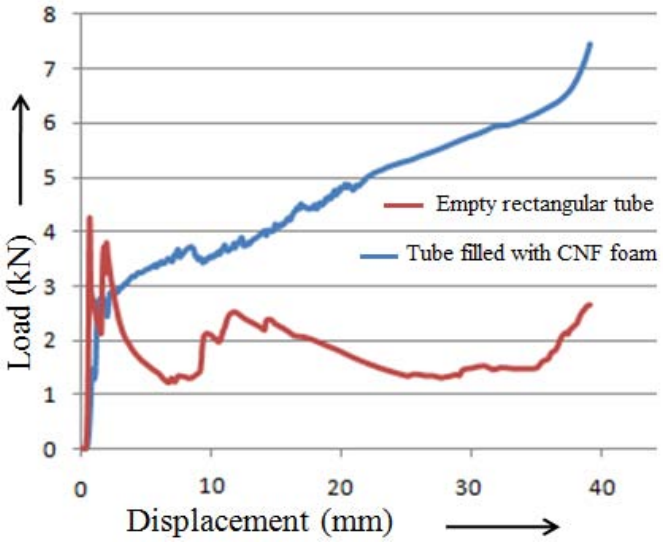

Figure 6.7 Load v/s displacement for empty and CNF filled steel tube

From the simulations, crushing patterns of empty steel tube and steel tube filled with CNF, at different stages of axial crushing are plotted in Figure 6.8. Folding patters of empty tube compared to CNF foam filled tube were abrupt, un-uniform and sudden. Whereas CNF foam filled tube crushes in more uniform, progressive and smooth pattern. Empty tube hardly produced two folds during crushing, but in case of CNF filled tube there were at least six folds are observed. CNF foam filling restrained the inward folding of the tube and thus produces more folds. This type of folding made the resultant structure much stiffer which ultimately improved the energy absorption capacity.

The results of this analysis were compared to the study conducted by Mamalis [5], where poly-urethane foam of different densities was used to fill the steel tube. Analysis was carried out to study its effects on energy absorption capacity and folding pattern.

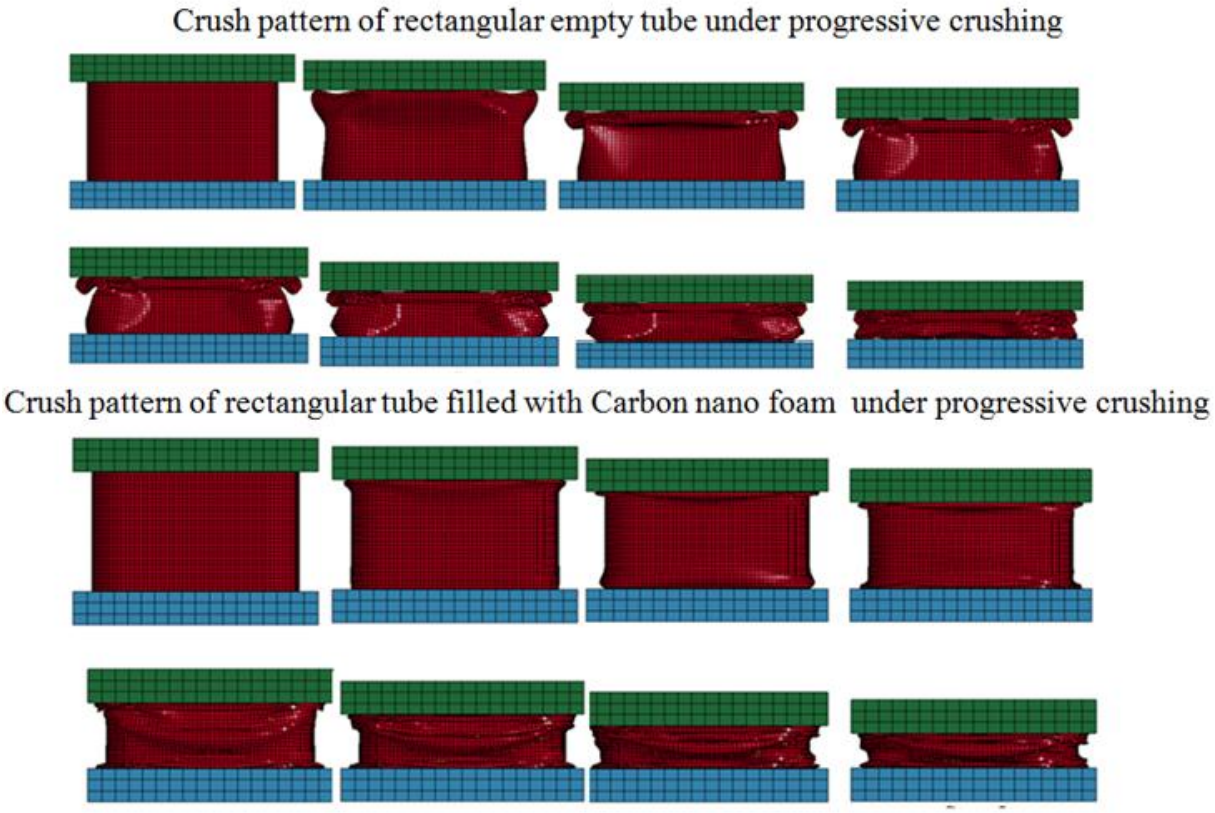

Figure 6.8 Crushing pattern of empty and CNF filled steel tubes

The comparison can be seen in the Figure 6.9. It is found that the energy absorbed by carbon nano foam is 14.5% more than the energy absorbed by the poly-urethane foam, figuratively steel tube filled with poly-urethane foam absorbed 158.5 J of energy, whereas CNF filled tube absorbed 181.0 J of energy. The crushing pattern of the tubes are almost the same but as the crushing distance increases the stiffness of the tube filled CNF foam increases more rapidly.

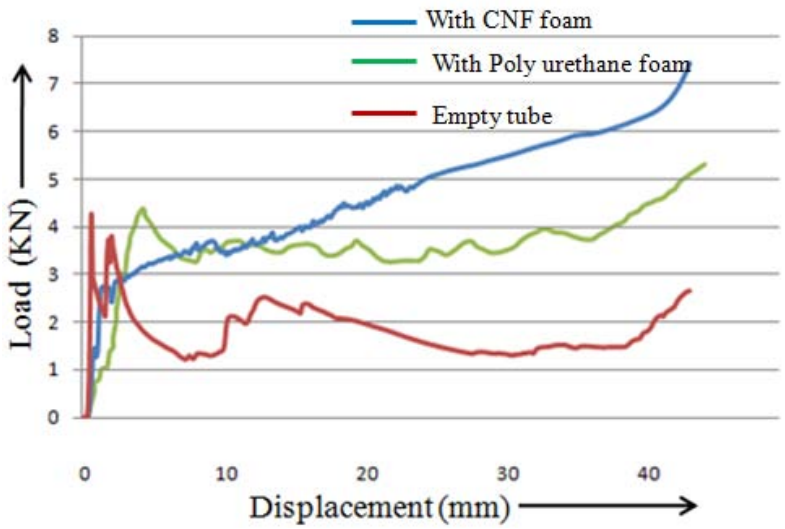

Figure 6.9 Load v/s displacements for empty, poly-urethane and CNF filled steel tube

Simulation results of load verses displacement and energy verses displacement curves of empty steel tube, poly-urethane foam steel tube and CNF foam filled steel tube are shown in Figure 6.9 and Figure 6.10. In the initial deformation region foam filling increases both peak load and mean load values. The load verses displacement curve slope of CNF increases sharply when compared to that of poly-urethane and empty tube.

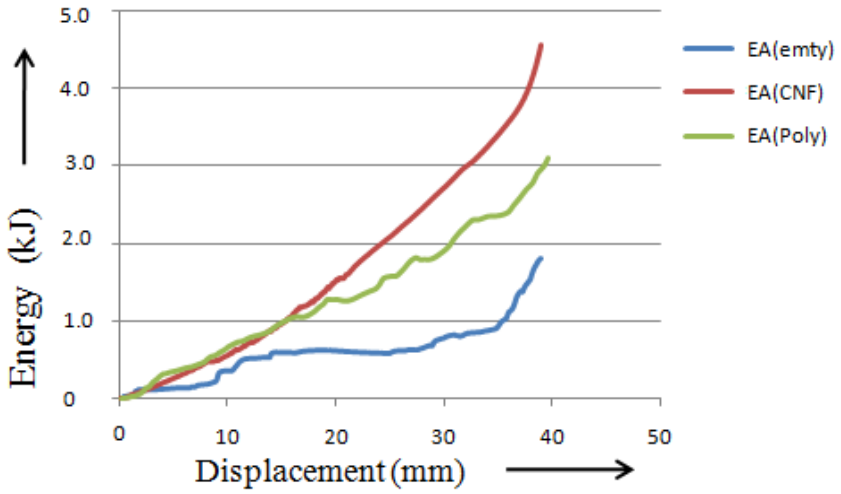

Figure 6.10 Energy Absorbed v/s displacements

The variation of mean load and SEA values of empty, po-urethane foam filled and CNF foam filled tubes are shown in Figure 6.10 and the results are tabulated in the Table 6.1. Table shows that there is significant amount increase in energy absorption, specially when the percentage of increase in energy absorption compared to empty steel tube to poly-urethane it is 122.0 % and to when compared to CNF foam filled tube it is 153.4 %.

Table 6.1 Summery of CNF energy absorption characteristics

Specimen	***Crush Length l (mm)***	***Peak Load*** P_{max} ***(kN)***	***Mean Load*** P_{mean} ***(kN)***	***Total Energy W (J)***	***SEA*** E_S ***(KJ/Kg)***	***% increase in Energy***
Empty	39	3.8	1.8	71.4	2.98	-
Poly-urethane	39	4.5	4.0	158.6	5.11	122.0
CNF	39	4.2	4.6	181.0	5.8	153.4

CHAPTER 7

BUMPER ANALYSIS OF DODGE CARAVAN

7.1 Dodge Caravan Finite Element Model Details

The Dodge Caravan model used in this study was developed by National Crash Analysis Center (NCAC), which is one of the leading research institutes for vehicle highway research and development [16]. In this case Dodge Caravan model is utilized to study the energy absorption characteristics of carbon nano foam. Dodge Caravan model was downloaded from national crash analysis center (NCAC) website. Researchers from NCAC developed this vehicle model and validated for the frontal impact conditions at 30 mph, 35 and 40 mph speeds. The validation was done by comparing the resultant accelerations and total wall forces obtained from the FE model simulation to the National Highway Traffic Safety Administration New Car Assessment Program (NHTSA) (NCAP) tests results and concluded that the model is stable in full frontal rigid wall simulations [16].

This finite element model details such as, the number of nodes, number of elements created, number of parts created, number of rigid walls used, etc., are tabulated in the Table 7.1. Dodge Caravan vehicle model was used in this study, because this vehicle model has a typical foam material in its bumper area and in this analysis, this foam material property was changed to carbon nano fiber (CNF) foam. New model created was then analyzed in frontal crash and bumper crash analysis.

Figure 7.1 shows the finite element model of Dodge Caravan vehicle, where one can observe that the fine mesh was used in front portion of the vehicle and coarse mesh in the later portion. This type of meshing not only reduces the analysis time but also the time and cost required for developing these FE models, without compromising on accuracy of the simulation

results. The different mesh sizes were used to reduce the simulation time, without s was was fine. In most of the frontal crash events, vehicle generally undergo significant deformation in case of frontal impacts; hence the frontal portion of most of the FE models which were developed for frontal impact were finely meshed and whereas the rear, and central rear portions are meshed with coarse mesh. Figure 7.1 shows the finite element model of Dodge Caravan, and the three rigid walls (Ground, and load cells of different stiffness values).

Table 7.1 Finite element details of Dodge Caravan model

Number of shell elements created	327199
Number of solid elements created	6253
Number of material cards used	511
Number of Nodes created	344774
Number of parts created	546
Number of rigid walls used	3
Number of sections created	511
Number of node sets created	1281
Number of part sets created	5

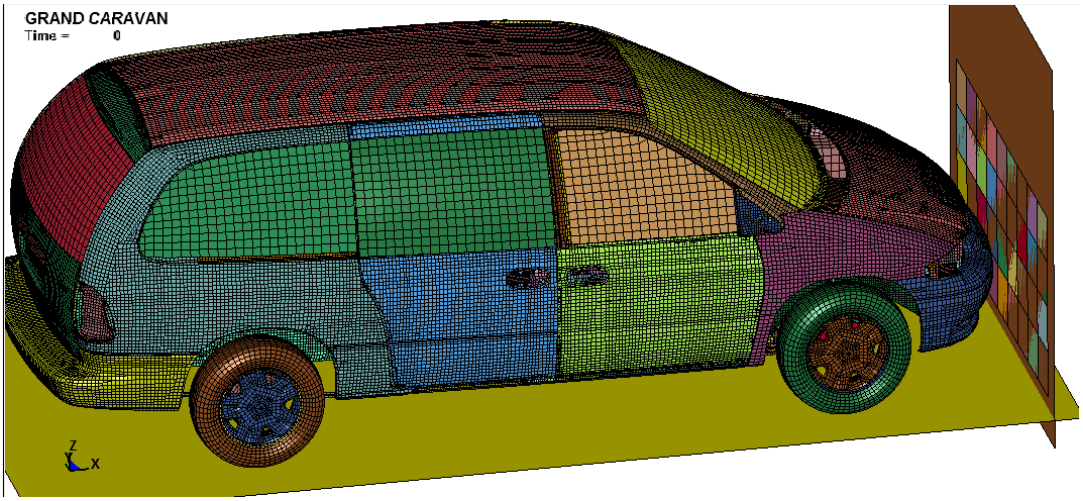

Figure 7.1 Finite element model of Dodge Caravan

To check the accuracy of the finite element model, the actual physical models data was compared with virtual physical model, these details are tabulated in Table 7.2.

Table 7.2 NCAP Comparison of dodge caravan model

	FE Model	***Test vehicle***
Weight (Kgs)	2043	2003
Engine Type	3.8L V6	3.3L V6
Tire size	P215/65 R15	P215/65 R15
Attitude (mm) As delivered	F-798	F-769
	R–846	F-766
Wheelbase (mm)	3030	3030
CG (mm)	1320	1319

7.2 Development of the FE Model

The FE model for this study is developed by changing the material model and its material properties of foam in bumper area as shown in Figure 7.2. This also shows the locations of accelerometers placed in the vehicle model. This can be done by using pre-processors like Hypermesh or Ls-Prepost. To check the accuracy of the new model, it is submitted Ls-Dyna.

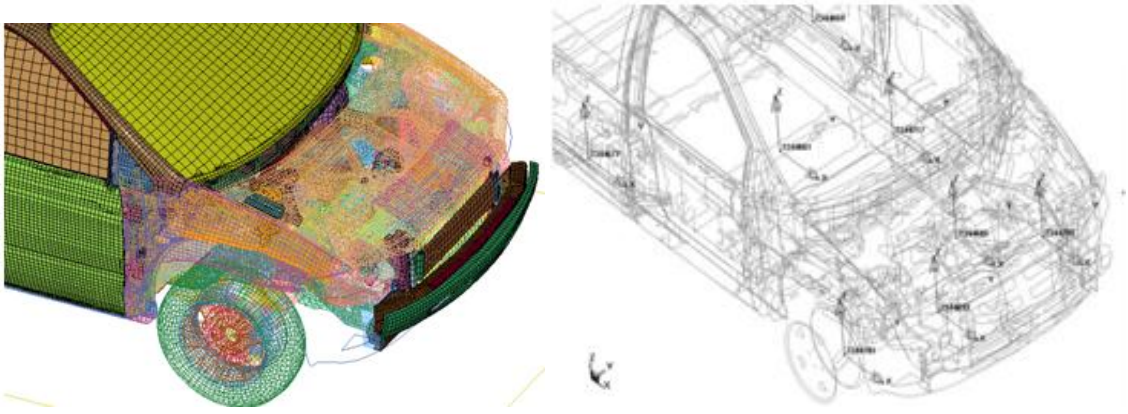

Figure 7.2 Modified bumper model and different accelerometer locations

In this study accelerations form different locations, specially the vehicle c.g, left seat and right seat nodal values of the vehicle model are used. These nodal locations and their names are tabulated in Table 7.3.

Table 7.3 Accelerometer locations in FE dodge caravan model 16]

Accelerometer Location	*Accelerometer Node Number*
Vehicle CG	2344661
Left seat	2344669
Right seat	2344677
Engine top	2344685
Engine bottom	2344693
Right brake caliper	2344701
Left brake caliper	2344709

7.3 Analysis of Dodge Caravan Model in Frontal Impact

In this study, the Dodge Caravan vehicle model was simulated at 35 mph and 10mph in full width frontal impact. The speeds 35 mph and 10 mph are selected to compare the results obtained from this study to the observations made to NHTSA NCAP test and bumper test conditions. A typical frontal impact is shown in Figure 7.3, where according to NCAP regulation in US, the vehicle is impacted to a rigid wall with a given speed of 30, 35, and mph [12]. The observations are made to asses different injuries of the passenger or driver.

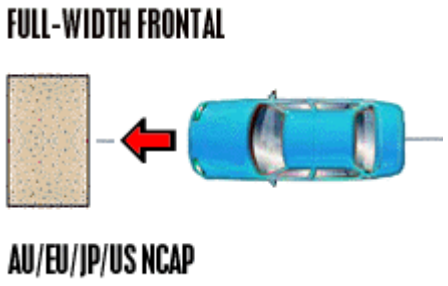

Figure 7.3 A typical frontal impact test set up [12]

7.3.1 Analysis of Dodge Caravan impact at 35 Mph

In this case, the modified Dodge Caravan vehicle model was impacted to rigid wall with an initial velocity of 35 Mph. The simulation was carried out for 0.1 sec and the accelerations from different locations are taken for the analysis. Figure 7.4, drawn for different stages of the vehicle interaction with rigid wall in full frontal impact scenario, showing the crushing behavior of the foam material.

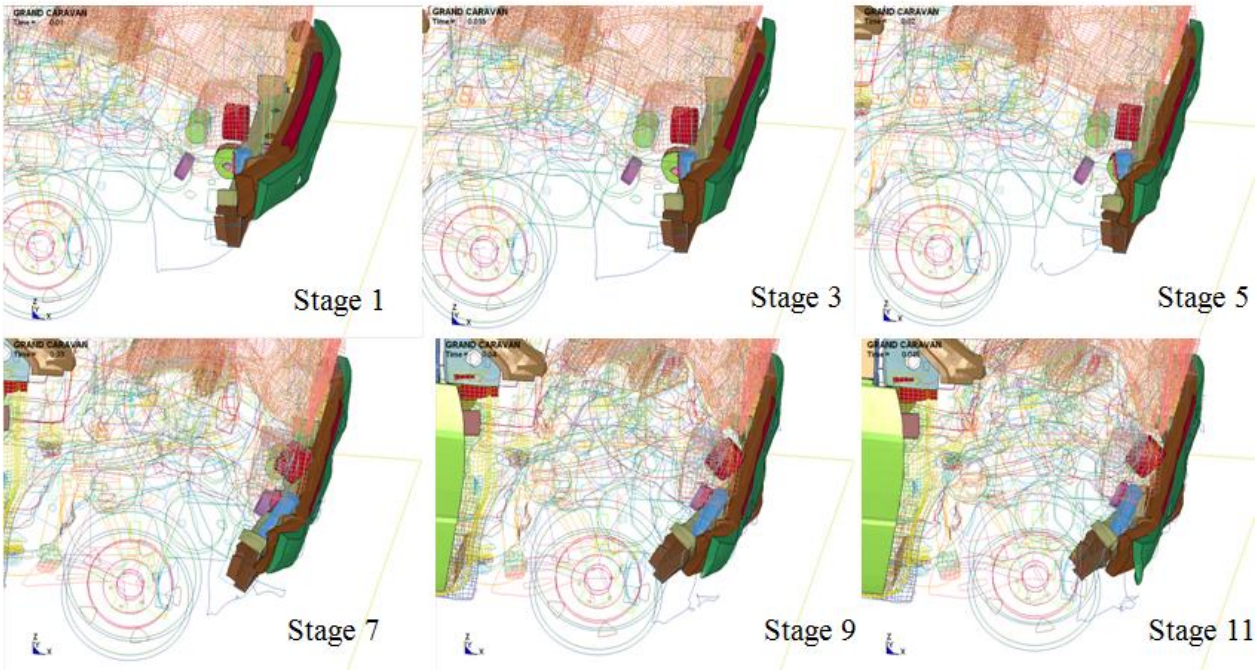

Figure 7.4 Stages of Dodge Caravan vehicle with carbon nano foam

The resultant accelerations from different locations of this analysis are compared with the corresponding resultant acceleration of the original FE model. Figure 7.5 (a) and (b) shows the acceleration plots (G's) drawn from left seat and right seat locations at 35 Mph. The observation are made and found that, by using carbon nano foam material there was a drop in transmitted acceleration (G's) to the either of seat locations. Quantitatively, about 15 G's accelerations were (approximately 15%) reduced.

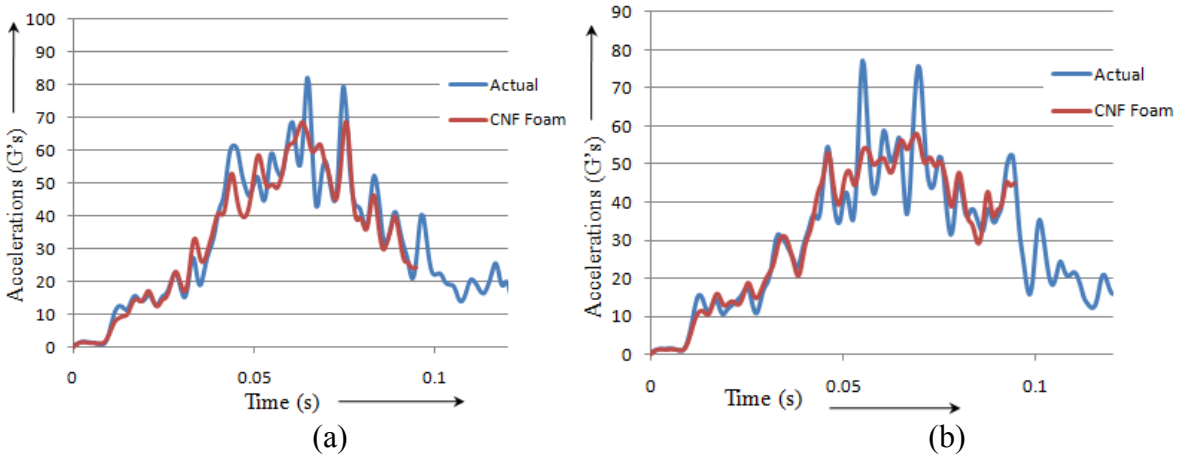

Figure 7.5 (a) Left seat accelerations at 35 mph (b) Right seat accelerations at 35 mph

7.3.2 Analysis of Dodge Caravan impact at 10 mph

In this case, the modified vehicle model was impacted to the rigid wall with an initial velocity of 10 Mph (approximately 15 kph). This particular speed is selected to observe the CNF foam behavior as in case of a bumper test. The simulation was carried out for 0.15 sec and the accelerations from different locations are taken for the analysis. The resultant acceleration results were drawn in terms of G's and plotted against the original FE model resultant acceleration. Figures 7.6, Figure 7.7 (a) and (b) shows the corresponding plots drawn for different locations namely, center of gravity, left seat location and right seat locations. The results obtained are compared, and it is observed from Figure 7.6; the application of CNF in the bumper area reduced the transmitted 5 G's of acceleration to vehicle center of gravity and approximately 3 G's in case of left seat (Figure 7.7 (a)). In case of right seat location referring Figure 7.7 (b), there was not much reduction observed in G's transmitted. However, there was shift in G's transmitted form 0.05 seconds to 0.09 seconds.

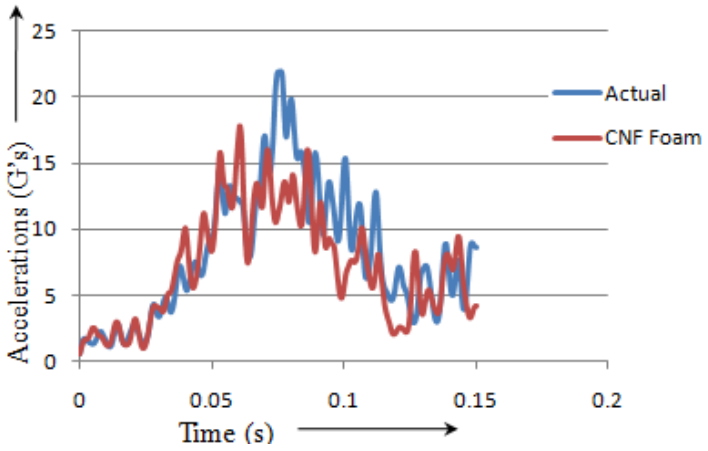

Figure 7.6 Center of gravity accelerations at 10 mph

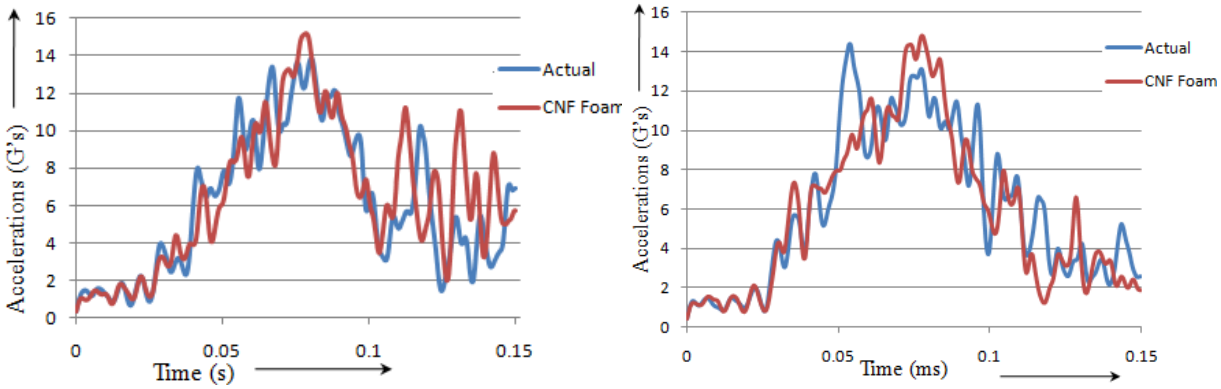

(a) (b)

Figure 7.7 (a) Left seat accelerations at 10 mph (b) Right seat accelerations at 10 mph

From the analysis conducted for two different speeds, it was evident that by using carbon nano foam material, there was a significant reduction in accelerations (G's) transmitted to the different vehicle part. Hence, one can conclude that CNF foam material absorbed the crash kinetic energy in frontal impact by undergoing significant deformation.

CHAPTER 8

CONCLUSIONS AND RECOMMENDATIONS

8.1 Conclusions

In this thesis, a thin-walled steel tube was used to study the effects of poly-urethane foam infused with carbon nano fibers on the energy absorption capabilities of the resultant structure. First, compression tests were carried out on different percentages of CNF foam material to study the effect of CNF infusion. Saha et al., CNF foam experimental data was used to obtain the numerical model. Non-linear FE models of the tube along with the foam were then developed in Ls-Dyna. The FE simulation of thin walled steel tube filled with CNF foam was analyzed and compared with the experimental work conducted by Mamalis et al [7]. Application of CNF foam in the bumper area of a Dodgde Caravan vehicle was then analyzed.

In this study the effects of infusion of carbon nano particles into poly-urethane foam were studied, and from the results, the fallowing conclusions are made

- The CNF foam filled thin-walled steel tube, mean load has improved when compared to empty steel tube and tube filled with poly urethane foam.
- The steel tube filled with carbon nano foam has better energy absorption (182 J) capability than empty steel tube (72 J).
- The energy absorption capability of the steel tube filled with carbon nano foam (182 J) was found to be 14.0 % better than the tube filled with typical poly-urethane foam(159 J).
- The progressive crushing behavior can be observed in steel tube filled with carbon nano foam.
- The specific energy absorption capacity of steel tube filled with CNF (6.0) is almost twice that of empty tube (3.0), and it is 20 % more than that of poly-urethane foams (5.0)

- In the full frontal crash simulation at 35 mph, 15 G's of accelerations reduction was observed, which is about 15 % reduction in G's.
- In case of 10 mph bumper analysis, about 2 G's of reduction was observed.

8.2 Recommendations for Future Study

Based on the conclusion made in this study, further research can be conducted using carbon nano foam in automotive, aviation or in any other transportation industry. Some of the primary and most significant applications of this thesis work are as follows.

- Further analysis can be carried out to determine the effect of change percentage change in weight of the carbon nano tubes on poly-urethane properties at different strain rates
- To consider strain-rate effects, experiments should be conducted at different speeds; i.e., strain rates and loads and thus utilizing these results analysis can be carried out using updated material models available in Ls-Dyna.
- The application of these foam materials can be analyzed by using foam material as padding material the automobile to study their behavior.
- Head impact tests, pelvic impactor tests can be performed to study the behavior of the CNF when it is used as padding material in automobile.
- The economical aspects of CNF foams applications in automotive industry would also be of interest.

REFERENCE

REFERENCES

[1] Mamalis A.G., " Crashworthiness of composite thin-walled structural components," Technomic Publishing Company, Inc., Lancaster, 1989.

[2] Du B. P., Chou C.; Khalil B., King A., Mahmood H., Mertz J., Wismans J., "Vehicle crashworthiness and occupant protection," American Iron and steel institute, 2004.

[3] Shetty S.S., "Finite element modeling of energy absorption characteristic of hybrid structure - composite wrapped on a square metal tube," MS Thesis, Wichita State University, USA 2006.

[4] Buckling of Columns, Panels and Shafts, http://www.grantadesign.com/resources/shapes/solutions/buckling.htm [cited 2011].

[5] Mamalis, A. G. , Manolakos, D. E. , Ioannidis, M. B. , Spentzas, K. N. and Koutroubakis, S. "Static axial collapse of foam-filled steel thin-walled rectangular tubes: experimental and numerical simulation," *International Journal of Crashworthiness*, Vol. 13, Issue 2, pp 117-126, April 2008.

[6] DeLorean URL: http://antholonet.com/EngineersCars/DeLorean/delorean.html [cited 2011].

[7] Saha, M.C., Kabir, Md.E., Jeelani, S., "Enhancement in thermal and mechanical properties of polyurethane foam infused with nanoparticles," *Material Science and Engineering*, Vol 479, Issues 1-2, pp 213-222, April 2008.

[8] Advanced compatibility engineering body structure," URL:http.automobiles.honda.com/certified-used/civic-hybrid/2007/safety.aspx [cited, 2011]

[9] Aljawi A.A.N., "Axial crushing of square steel tubes," The 6th saudi engineering conference 2002, Vol. 3, pp 3-18, 2002.

[10] Salehghaffari, S., Panahipoor, M., Tajdari, M., "Controlling the axial crushing of circular metal tubes using an expanding rigid ring press fitted on top of the structure," *International Jornal of Crashworthyness*, Vol. 1, Bolton, 2011.

[11] Hanefi EH, Wierzbicki T., "Axial resistance and energy absorption of externally reinforced metal tubes," *Composites part B,* Vol. 94, pp 270-387, 1996.

REFERENCES (Continued)

[12] Altenhof W., Harte A., Turchi R., "Experimental and numerical compression testing of aluminum foam filled mild steel tubular hat sections," 7th International Ls-Dyna users conference, pp 13-29, 2009.

[13] Material Specific Properties of Duocel® Foams, URL:ergaerospace.com/foamproperties/matspecificproperties.htm [cited 2010]

[14] LS-DYNA Keyword User's Manual, Version 960, Volume II, Livermore Software Technology Corp., Livermore, CA, 2000.

[15] Abramowicz, W. and Wierzbicki, T., "Axial Crushing of Foam-Filled Columns," *International Journal of Material Science*, Vol. 30, pp 263-271, 1988.

[16] National Crash Analysis Center, http://www.ncac.gwu.edu/, [cited 2010]

[17] Slik, G., Vogel, G., Chawda, V., "Material validation of a high efficient energy absorbing foam," 5th Ls-Dyna Forum, Material III Foams/Composites, Dow automotive, Materials Engineering Center, Germany, 2006.

[18] Berry J. P., "Energy Absorption and Failure Mechanisms of Axially Crushed GRP Tubes," Ph.D. Dissertation, University of Liverpool, UK, 1984.

[19] Florent P., Wenyi Y., Cui W., "Crushing Modes of Aluminum Tubes under Axial Compression," 5th Australasian Congress on Applied Mechanics, Australia, 2007.

APPENDIX

APPENDIX

The Ls-Dyna key words utilized in this study

```
$$ HM_OUTPUT_DECK created 21:45:45 05-22-2010 by HyperMesh Version 10.0build6
$$ Ls-dyna Input Deck Generated by HyperMesh Version  : 10.0build60
$$ Generated using HyperMesh-Ls-dyna 971 Template Version : 10.0build60
*KEYWORD
$$
$$ Units: mm, ms, Kg, GPa, Kn-m
$
*KEYWORD
$
*TITLE
Steel tube
$
*CONTROL_TERMINATION
$$  ENDTIM    ENDCYC     DTMIN    ENDENG    ENDMAS
      68.0         0       0.0       0.0       0.0
$
*DATABASE_HISTORY_NODE
$       id1         id2         id3         id4         id5         id6         id7
id8
$...>....1....>....2....>....3....>....4....>....5....>....6....>....7....>..
..8
        50         40         57         67         63         46         72
$
*CONTROL_ENERGY
$$    HGEN      RWEN    SLNTEN     RYLEN
         2         2         2         1
$
*DATABASE_GLSTAT
$#      dt    binary
  0.500000         1
$
*DATABASE_MATSUM
$#      dt    binary
  0.500000         1
$
*DATABASE_NODOUT
$#      dt    binary
  0.100000         1
$
*DATABASE_RCFORC
$#      dt    binary
  0.100000         1
$
*DATABASE_SLEOUT
$#      dt    binary
  0.100000         1
$
*DATABASE_BINARY_D3PLOT
$$ DT/CYCL      LCDT      BEAM     NPLTC
$#      dt      lcdt      beam     npltc
  1.000000
```

```
$#   ioopt
         0
$
*DATABASE_BINARY_D3THDT
$$ DT/CYCL      LCID
$#      dt      lcdt  not used  not used
         1
$
*DATABASE_EXTENT_BINARY
$HMNAME MATS       2BOTTUM
$#    neiph      neips     maxint     strflg     sigflg     epsflg     rltflg
engflg
         0          0          0          0          0          0          0
0
$HMNAME MATS       2BOTTUM
$#   cmpflg     ieverp     beamip      dcomp       shge      stssz     n3thdt
ialemat
         0          1          0          0          0          0          0
0
$HMNAME MATS       2BOTTUM
$# nintsld   pkp_sen      sclp    unused     msscl     therm
         0          0     0.000         0         0         0
*PART
$HMNAME COMPS       1box
$HWCOLOR COMPS       1      11

         1         1         1
$
$
*PART
$HMNAME MATS       2BOTTUM
$# title

$#     pid     secid       mid
         2         2         2
$
*PART
$HMNAME MATS       3top
$# title

$#     pid     secid       mid
         3         2         3
$
*MAT_RIGID
$HMNAME MATS       3top
$#     mid         ro          e         pr          n     couple          m
alias
         3 7.8000E-6 2.1000E+2  0.300000     0.000     0.000     0.000
$#     cmo      con1      con2
  1.000000         6         7
$#lco or a1       a2        a3        v1        v2        v3
     0.000     0.000     0.000     0.000     0.000     0.000
$
$
$
*MAT_RIGID
$HMNAME MATS       2BOTTUM
```

```
$#      mid         ro          e          pr          n     couple          m
alias
         2 7.8000E-6 2.1000E+2  0.300000     0.000     0.000     0.000
$#     cmo      con1      con2
  1.000000         7         7
$#lco or a1       a2        a3        v1        v2        v3
     0.000     0.000     0.000     0.000     0.000     0.000
$
$
*MAT_PIECEWISE_LINEAR_PLASTICITY
$HMNAME MATS       1MSteel335
         17.8300E-06      207.0         0.3      0.210         1.0         0.0
0.0
       0.0       0.0         0         0       0.0
$$ HM Entries in Stress-Strain Curve =0
*MAT_CRUSHABLE_FOAM
$$     MID         RO          E           PR         LCID
        4   5.8166e-06     18503           0          63          0.3
*DEFINE_CURVE
63,,1,1
0,0
0.00465,7.07315
0.00787,17.7883


0.01439,139.297
0.01519,148.4633


$
*SECTION_SHELL
$HMNAME PROPS       1shell
         1          2        1.0          3        0.0        0.0          0
1
       0.3        0.3        0.3        0.3        0.0        0.0        1.0
0
$
$
*SECTION_SOLID
$HMNAME PROPS       2solid
         2         1         4
$
*CONTACT_AUTOMATIC_SINGLE_SURFACE_ID
$HMNAME GROUPS       1cir
$HWCOLOR GROUPS       1      11
         1
         1                     3                       0          0          0
0
       0.3          0.2          0.0          0.0          0.0             0
0.01.0000E+20
       1.0        1.0        0.0        0.0        1.0        1.0        1.0
1.0
$
$
*CONTACT_AUTOMATIC_NODES_TO_SURFACE_ID
$HMNAME GROUPS       1solid2ube
$HWCOLOR GROUPS       1       2
```

```
         2
         1           2           3           3           0           0           0
0
       0.3           0.2           0.0           0.0           0.0             0
0.01.0000E+20
       1.0         1.0         0.0         0.0         1.0         1.0         1.0
1.0
$
$
*CONTACT_AUTOMATIC_NODES_TO_SURFACE_ID
$HMNAME GROUPS       2solid2tube
$HWCOLOR GROUPS       1       3
         2
         1           3           3           3           0           0           0
0
       0.3           0.2           0.0           0.0           0.0             0
0.01.0000E+20
       1.0         1.0         0.0         0.0         1.0         1.0         1.0
1.0
$
*BOUNDARY_PRESCRIBED_MOTION_RIGID
$HMNAME LOADCOLS       1rigidvel
$HWCOLOR LOADCOLS       1       7
         3           2           0           2       -0.5           01.0000E+28
0.0
$#      pid         dof         vad       lcid          sf         vid      death
birth
$
*DEFINE_CURVE
$#    lcid      sidr       sfa       sfo      offa      offo    dattyp
         2         0  1.000000  1.000000
$#                a1                  o1
          0.01000000          0.00205000
          0.03000000          0.00421889


          0.97000003          0.99777675
          0.99000001          0.99975187
          1.00999999          0.99975473
         10.00000000          1.00000000
        100.00000000          1.00000000
        1000.0000000          1.00000000
*NODE
      13            31.5             0.0           -24.5
      14            31.5             2.0           -24.5
      15            31.5             4.0           -24.5

   11093 0.5027238905449            54.0 -6.446705503312
   11094 4.3865882226868            54.0 -6.479344179538
   11095  8.176129629028            54.0 -6.566160908464
   11096 11.871583017593            54.0 -6.778107576295
*ELEMENT_SHELL
       1       1     197     199     201     196
       2       1     196     201     192     193
       3       1     199     200     202     201
```

```
    3562       1    3708    3707    3688    3687
    3563       1    3698    3704    3708    3699
    3564       1    3704    3703    3707    3708
*ELEMENT_SOLID
    3781       2     3807     3805     3804     3809     3967     3970     3969
3968
    3782       2     3809     3804     3801     3800     3968     3969     3972
3971


   3785       2     3793     3810     3799     3794     3974     3975     3978
3977
    3786       2     3810     3809     3800     3799     3975     3968     3971
3978
*END
```